OULUN YLIOPISTO
UNIVERSITY of OULU

DEGREE PROGRAMME IN ELECTRICAL ENGINEERING

MASTER'S THESIS

WIRELESS MAINS SENSOR FOR MONITORING DOMESTIC ENERGY CONSUMPTION

Author	Jani Ylioja
Supervisor	Timo Ojala
Second Examiner	Kari Määttä

November 2014

Ylioja J. (2014) Wireless Mains Sensor for Monitoring Domestic Energy Consumption. Department of Electrical Engineering, University of Oulu, Oulu, Finland. Master's thesis, 61 p.

ABSTRACT

Past studies have shown that awareness of energy consumption can lead to reduction in electricity usage and that real-time, per-appliance data on electricity consumption would provide greater utility and actionable information. Yet, the customers of today's utility companies typically have to be content with data that is aggregated, delayed and difficult to access. Comprehensive real-time data would also aid in optimizing energy consumption with respect to dynamic pricing and avoiding peak consumption periods.

The objective of this thesis was to design and manufacture a wireless sensor for continuous and real-time metering of the energy consumption of a household in the UBI-AMI system version 2. The resulting Mains sensor reads the total energy consumption from the kilowatt hour meter using either a galvanic or an optical connection. The individual loads of the fuses in the circuit breaker panel are measured with Hall sensors. An 8-bit microcontroller collects analog measurements, conducts 10-bit ADC and transmits the resulting digital data to the UBI-AMI system using a commercial 6LoWPAN radio module and the CoAP protocol. The data enables the differentiation of the energy consumption of integrated and built-in elements such as floor heating and sauna from the total energy consumption of the household.

The Mains sensor was tested with a demonstrator that comprised of a fuse board, a kilowatt hour meter and sockets for connecting loads. The Mains sensor was found to be flawless in reading the total energy consumption from the kilowatt hour meter using a galvanic connection. The sensor was able to read 84% of fast pulses and showed 4% surplus with slow pulses if the optical connection was used. The Hall sensors had a maximum average error of 0.47% with an active power, in comparison to a commercial energy meter. These results show that the Mains sensor provides sufficiently accurate and reliable information for improving the awareness of energy consumption of a household.

Keywords: Hall sensor, smart energy meter, Wireless Sensor Network, CoAP, 6LoWPAN

Ylioja J. (2014) Langaton sähköpäätaulusensori kotitalouden energiankulutuksen seuraamiseen. Oulun yliopisto, sähkötekniikan osasto. Diplomityö, 61 s.

TIIVISTELMÄ

Tutkimusten mukaan tietoisuus energiankulutuksesta voi johtaa sähkön käytön vähenemiseen, ja että tosiaikainen, laitekohtainen kulutustieto olisi hyödyllisempää. Silti nykyisin sähköyhtiöiden asiakkaiden täytyy tyypillisesti tyytyä kulutustietoihin, jotka on kerätty kokonaiskulutuksesta, ovat käytettävissä viiveellä, ja joihin on vaikea päästä käsiksi. Kattava tosiaikainen informaatio myös auttaisi huippukulutuskausien välttämisessä ja energiankulutuksen optimoinnissa dynaamisen hinnoittelun suhteen.

Tämän diplomityön tavoitteena oli suunnitella ja valmistaa langaton sensori kotitalouden energiankulutuksen jatkuvaan ja tosiaikaiseen mittaukseen osana UBI-AMI-järjestelmän versiota 2. Syntynyt sähköpäätaulusensori lukee kokonaisenergiankulutuksen kilowattituntimittarista joko galvaanista tai optista yhteyttä käyttäen. Yksittäiset ryhmäkohtaiset kuormat mitataan sulaketaulusta Hallin antureilla. 8-bittinen mikrokontrolleri kerää analogiset mittaukset ja muuntaa ne digitaaliseksi dataksi, joka lähetetään UBI-AMI-järjestelmälle käyttäen kaupallista 6LoWPAN-radiomoduulia ja CoAP-protokollaa. Mittausdata mahdollistaa integroitujen ja kiinteästi asennettujen sähkölaitteiden, esimerkiksi lattialämmityksen ja saunan, energiankulutuksen eriyttämisen kotitalouden kokonaiskulutuksesta.

Sähköpäätaulusensorin toiminta arvioitiin testilaitteistolla, joka koostui sulaketaulusta, kilowattituntimittarista ja pistorasioista kuormien liittämistä varten. Sähköpäätaulusensorin havaittiin lukevan kokonaisenergiankulutuksen kilowattituntimittarista virheettömästi galvaanista yhteyttä käyttäen. Optista yhteyttä käytettäessä sensori kykeni lukemaan 84% nopeista pulsseista ja hitaat pulssit saivat sensorin mittaamaan käytetyn energian 4% todellista suuremmaksi. Hallin antureilla suurin keskimääräinen virhe kaupalliseen mittariin verrattuna oli 0,47% pätötehollisella kuormalla. Tulosten perusteella sähköpäätaulusensori antaa riittävän tarkkaa ja luotettavaa tietoa energiankulutuksesta ja sitä voidaan käyttää energiankulutuksen tietoisuuden lisäämiseen kotitalouksissa.

Avainsanat: Hall-anturi, älykäs energiankulutusmittari, langaton sensoriverkko, CoAP, 6LoWPAN

CONTENTS

FOREWORD

This master's thesis was done at the University of Oulu, Department of Computer Science and Engineering, MediaTeam Oulu research group. The aim was to design a device for measuring the real time energy consumption of individual circuit breakers in a circuit breaker board as well as kilowatt hour meter via a wireless sensor network, to enable consumer-level measurement of energy consumption and to increase awareness of energy usage. I would like to thank my supervisor and long-term employer Professor Timo Ojala for the opportunity for this thesis and for his support during the work. I would also like to thank the second supervisor University Lecturer Kari Määttä especially for sharing his great knowledge on analogue electronics, as well as my colleagues in MediaTeam. Finally, many thanks to the Oulun Sähkömyynti for the scholarship of the Pohjoista Voimaa Energiatili, and to Production Manager Matti Lehto at Oulun Energia and Energy Adviser Jarmo Meriläinen at Oulun Sähkömyynti for their expert assistance.

Oulu, October 30, 2014

Jani Ylioja

ABBREVIATIONS

6LoWPAN	IPv6 over Low power Wireless Personal Area Networks
AC	Alternating Current
ADC	Analog to Digital Converter
ALU	Arithmetic Logic Unit
AMI	Automated Metering Infrastructure
AMR	Anisotropic Magnetic Resistance
ANSI	American National Standards Institute
API	Application Programming Interface
ASIC	Application Spesific Integrated Circuit
BS	Base Station
CMR	Colossal Magnetic Resistance
CoAP	Constrained Application Protocol
CoRE	Constrained RESTful Environments
CSMA/CA	Carrier Sense Multiple Access With Collision Avoidance
CSMA/TDMA	Carrier Sense Multiple Access / Time Division Multiple Access
DC	Direct Current
dSID	digitalSTROM Identification Device
DTLS	Datagram Transport Layer Security
EEPROM	Electronically Erasable Programmable Read-Only Memory
EMC	Electromagnetic Compatibility
EUI	Extended Unique Identifier
f_c	Cutoff Frequency
GMR	Giant Magnetic Resistance
GND	Ground
GPIO	General Purpose Input Output
HAN	Home Area Network
HEMS	Home Energy Management Systems
HP	High Pass
HTTP	Hypertext Transfer Protocol
HW	Hardware
IANA	Internet Assigned Numbers Authority
IC	Integrated Circuit
ICMPv6	Internet Control Message Protocol version 6
IDE	Integrated Development Environment
IID	Interface Identifier
IoT	Internet of Things
IP	Internet Protocol
IPv4	Internet Protocol version 4
IPv6	Internet Protocol version 6
IR	Infra Red
ISM	Industrial, Scientific and Medical radio bands
ISR	Interrupt Service Routine
JTAG	Joint Test Action Group
kWh	Kilowatt hour
LED	Light Emitting Diode

LNA	Low Noise Amplifier
LOS	Line of Sight
LP	Low Pass
LSB	Least Significant Bit
M2M	Machine to Machine
MAC	A Media Access Control
MCU	Micro Controller Unit
MPE	Maximum Permissible Error
MTU	Maximum Transmission Unit
OA	Operational Amplifier
OS	Operating System
OSI	Open Systems Interconnection Model
PAN	Personal Area Network
PC	Personal Computer
PCB	Printed Circuit Board
PLC	Power Line Communications
PoE	Power over Ethernet
PRIME	Powerline Intelligent Metering Evolution
RC-Filter	Resistor-Capasitor -Filter
RAM	Random Access Memory
ROM	Read Only Memory
REST	Representational State Transfer
RS232	Recommended Standard 232
RSS	Rich Site Summary
SMS	Short Message Service
SOAP	Simple Object Access Protocol
SoC	System on a Chip
SPI	Serial Peripheral Interface
SQUID	Superconducting Quantum Interference Device
SW	Software
UART	Universal Asynchronous Receiver-Transmitter
UBI	UrBan Interactions
UDP	User Datagram Protocol
UI	User Interface
URI	Uniform Resource Identifier
USART	Universal Synchronous/Asynchronous Receiver-Transmitter
VA	Voltampere, power
var	Var, Voltampere reactive power
Vcc	Circuit power supply
W	Watt, voltampere active power
WLAN	Wireless Local Area Network
WSN	Wireless Sensor Network
XML	Extensible Markup Language

1. INTRODUCTION

Despite numerous energy efficiency policies and programs electricity consumption continues to grow. In the EU-25 member states the consumption of the residential sector increased by 10.8% during the period of 1999-2004. In the USA the annual power consumption has tripled during the past two decades. Residential and commercial buildings contribute significant proportion of the total energy consumption, 54% in the EU-25 and 41% in the USA. Further, it has been estimated that 30% of that energy consumption is wasted. [1, 2, 3]

Past studies such as Chetty et al. [4] have proven that awareness of energy consumption in homes and offices can lead to up to 20% reduction in electricity usage. While Stern [5] showed a long time ago that real-time, per-appliance data on electricity consumption would provide substantially greater utility and actionable information, the customers of today's utility companies typically have to be content with data that is aggregated, delayed and difficult to access.

Electricity is distributed through a building along a tree-like structure called a load tree, where the root connects the building to the power grid and the leaves correspond to individual electric appliances. In an ideal case we would want to have a full, detailed and real-time view of the load tree by monitoring the aggregate load at the root (top-down view) and the individual loads at every appliance (bottom-up view).

We have earlier presented a system called the UBI-AMI version 1 for the real-time metering of energy consumption in a household. The Mains sensor measured the aggregate load and the Socket sensors measured individual loads of selected appliances. The sensors transmitted the data over a 2.4 GHz multi-hop IP-based WSN to a router which forwarded the data to a server[6]. The server created different representations of the data which could be viewed with a web-based user interface (UI) and downloaded as RSS feeds. The UI also allowed the user to turn individual sensors (i.e. appliances attached to them) on and off, and request email/SMS alarms based on sensor data. [7]

The goal of this thesis is to design and implement a new Mains sensor for the UBI-AMI version 2. The Main sensor would be capable of monitoring not only the aggregate load but also its components, i.e. fuse-group specific energy consumptions of a circuit board, to obtain more accurate information of the energy consumption. The Main sensor is to be connected to the kilowatt hour meter and to the distribution panel. The data is transmitted wirelessly to avoid unnecessary cables. The used frequency is 868 MHz which provides better range and penetration through walls than the 2.4 GHz frequency used in the UBI-AMI version 1. The Mains sensor can measure the consumption of, for example, sauna, stove, electric heating and hot water boiler and differentiate their energy consumption from the total consumption. The data reveals the impact of each integrated appliance to the energy economy of a house and it can be used to track down appliances that consume too much energy. The data also helps in setting room temperatures in case of electric heating or cooling.

This thesis is organized as follows. Chapter 2 discusses different technologies for measuring energy consumption and how wireless sensor networks can be used for collecting load measurements. Chapter 3 presents the design of the Main sensor, followed by implementation in Chapter 4. Chapter 5 reports the evaluation of the Main sensor and Chapter 6 concludes the thesis.

2. MONITORING OF DOMESTIC ENERGY CONSUMPTION WITH WIRELESS SENSOR NETWORKS

2.1. Load Tree

The structure used to distribute electricity in a building is called a load tree. Figure 1 shows a partial example of a load tree, where the root connects the building to the power grid through the kilowatt hour meter. Main fuses, one for each phase of the three phase alternating current (AC), correspond to bigger branches. They are divided further to smaller branches of fuses that have a group of leaves denoting individual electric appliances. To gain all the information about the load tree we would have to have a full, detailed and real-time top-down view as well as bottom-up view of the load tree. However, this is rarely possible in practice due to cost and scalability issues, when a building contains hundreds or thousands of appliances or some of the appliances are not easily accessible. [7]

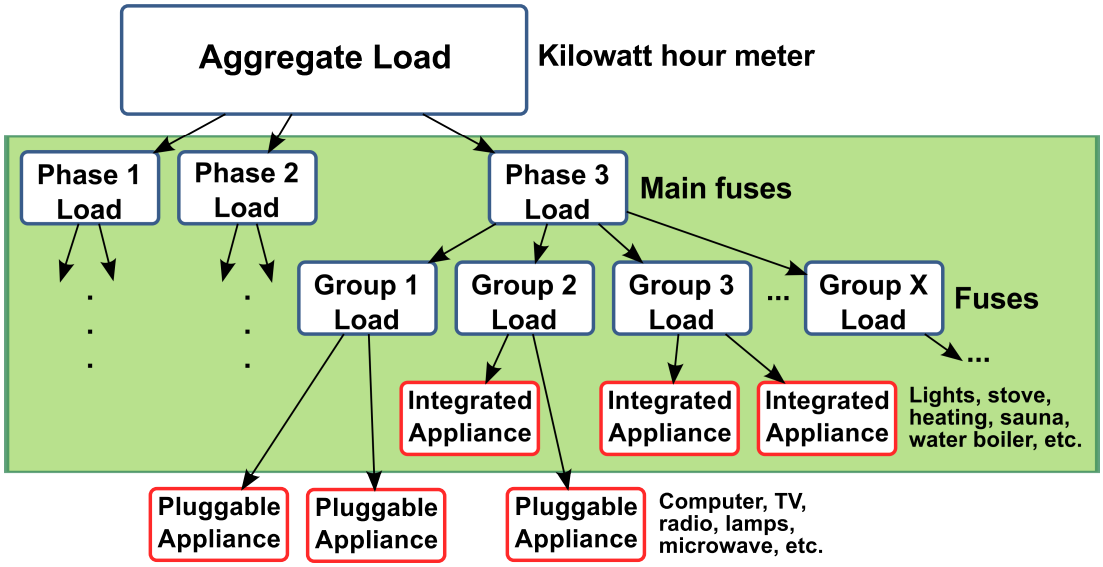

Figure 1. Load Tree: Aggregate load is on the top. Green area is unaccessible to the pluggable energy meters and to root load electricity meter.

Numerous academic and industrial approaches have been proposed for monitoring appliance level loads, for example the MIT Plug for profiling a load over short and long time scales[8]. Many startups have introduced wireless energy monitoring solutions based on ZigBee technology [9]. These products provide detailed power measurements of selected individual loads, which contribute to the bottom-up view of the power consumption.

Reactive and real power signatures of appliances can be employed for disaggregating individual loads from the aggregate load as originally proposed by Hart and later refined by many studies[10]. This approach is feasible for a small number of loads that have distinguishable differences in power signatures.

By monitoring the load at the root a top-down view of the load tree can be pursued. Many utility companies have introduced AMI (Automated Metering Infrastructure)

solutions that provide almost real-time data on the aggregate energy consumption of homes. Aggregators such as the Google PowerMeter and the Microsoft Hohm, both recently discontinued, provide more detailed feedback on energy consumption at a household level[11, 12]. Fortum Kotinäyttö includes a handheld device in monitoring aggregate load in kilowatt hours or in euro [13]. For new buildings KNX type integrated home automation or similar could be installed and Powerline Intelligent Metering Evolution (PRIME) could be used to communicate with the utility company, in addition to IP-based protocols[14, 15].

2.2. Technologies for Measuring Current

There are different ways to measure current, voltage and energy consumption. Their relative properties such as the requirement to have a galvanic connection to the subject of the measurement, output signal type, accuracy and operational temperature are essential for designing functional input circuitry to the Mains sensor.

2.2.1. Shunt Resistor

Current can be measured by measuring decrease in voltage over a shunt resistor (Figure 2). If the power of a reactive load is to be measured, then the phase shift between voltage and current must also be observed. Energy consumption is determined by integrating the product of voltage and current over the time period of the measurement. In modern meters this is achieved by using special application specific integrated circuits (ASIC). [16]

For example, Motorola's MCP3909 circuit can be configured via SPI-bus to provide the active electricity of the measurement as pulses to the pulse output or as values from the circuit's multiplier or the current and voltage values can be read directly from the circuit's analog to digital converters (ADC) [17].

Figure 2. A piece of metal used as a shunt resistor in a cheap commercial energy meter.

2.2.2. Hall Sensors

The Hall effect caused by the Lorenz force can be observed as a voltage difference because it makes a current flowing in an magnetic field to deviate from the original direction. The voltage difference is observed parallel to the deviation. The principle of a Hall sensor is shown in Figure 3. The Hall effect was originally discovered by Edwin Hall with a thin plate of gold. Later, the Hall effect has been found out to be stronger on semiconductors. Even though most Hall sensors are used to detect if a magnetic counterpart is nearby, yet some of them are specifically designed for measuring current. A Hall sensor is fed with constant current and any deviation in the magnetic field denotes voltage difference. [18, 19]

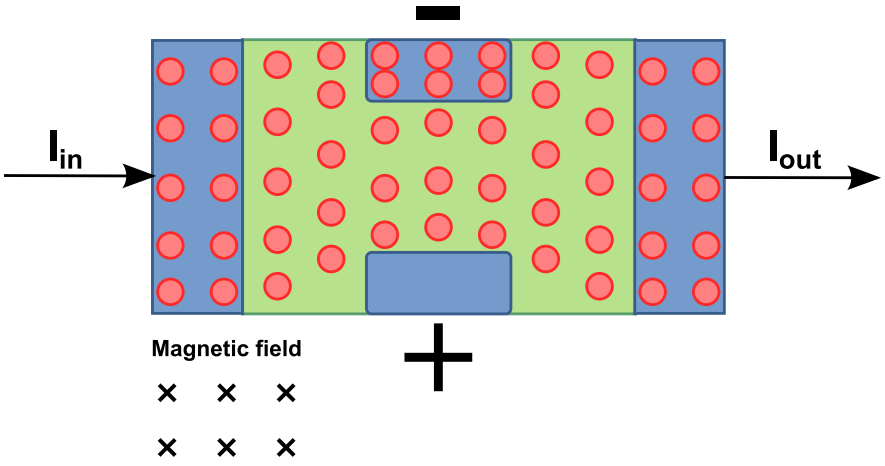

Figure 3. The principle of the Hall sensor: the magnetic field forces electrons to deviate from the straight line between the up and down of the conducting pad causing voltage difference which is directly proportional to the strength of the current.

The advantages of Hall sensors include:

1. There is no need for a galvanic connection to the observed subject unless voltage is also measured;
2. No common mode voltage to complicate the design of the meter circuit;
3. No voltage digression typical to shunt resistors thus no significant loss of energy.

Particularly, the lack of the galvanic connection to the subject of the measurement is a great advantage when high voltages are measured. A Hall sensor allows using a regular power supply and having the whole measurement circuit at safe voltages without the risk of electric shock. A disadvantage is that the measurement of mere current facilitates calculating only apparent power. The accuracy of the Hall sensor can be improved and the sensitivity to the external noises can be reduced by placing a high permeability path to the magnetic flux around the current conductor, for example a ferrite toroid. The ferrite must be entirely cut where the Hall sensor is installed, in order not to have magnetic flux bypass the sensor through the ferrite path. Also, the

measured conductor must be installed as close to the center of the ferrite as possible, to avoid leakages of magnetic flux from the ferrite. The sensitivity can be improved using toroid shaped materials with permeability, and by making thin gaps for the sensing parts to the toroids and looping the current conductor several times through the toroid. There are both closed loop and open loop versions among the "off the shelf" integrated Hall sensors. The closed loop sensors have negative feedback circuitry implemented by coil around the toroid that can be fed with current in desired ratio according the normal negative feedback theory in order to reduce the errors of linearity and/or amplification of the result. An example of the Hall sensor is shown in Figure 4.

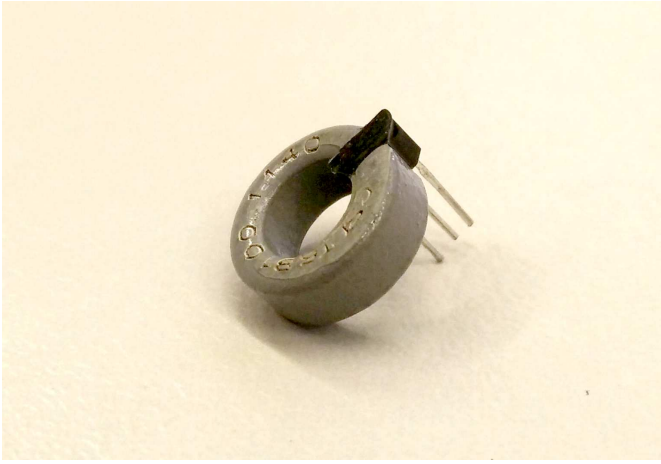

Figure 4. An analog open loop Hall sensor.

2.2.3. Current Transformer

Modern current transformer sensors are based on the same principle of measuring magnetic field around a current conductor as in Hall sensors. Further, same techniques can be used for improving accuracy and reducing noise. Main differences are that a current transformer does need operating voltage since coil is a passive component, and its inability to measure direct current (DC). The signal output of a current transformer can be either voltage or current. The measurement is carried out over a parallel laid resistor with the voltage output. In case of current signal there is a protection diode, for example in the SCT-13 series sensor heads to limit biggest power surges. The SCT-13 clip on type current transformer is presented in Figure 5. In terms of accuracy another drawback of using a coil as a sensor is that it has a tendency to resist any change in the current going through it. This causes phase error in the signal output. For example, the datasheets of ECHUN ECS1030-L72 measuring head gives a maximum value of 4 degrees for phase error [20]. This is not a problem if only current is measured, but it causes error in power measurements. Again, the measurement of a reactive power requires a galvanic connection to the subject of the measurement. This in turn requires paying attention to the safety issues if voltages exceeding safe levels are used. [21]

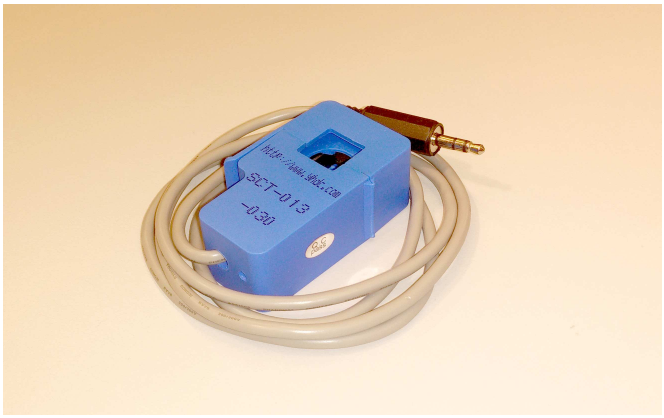

Figure 5. A clip on type current transformer.

An interesting subtype of transformer sensors is a Rogowski-coil. It is flexible and therefore can be installed in narrow spaces. Rogowski coils are used for example with mobile and handheld meters when measuring currents without galvanic connection. [16, 22]

2.2.4. Fluxgate Sensor

Flux gate sensors are based on the hysteresis of the permeability material. The material is driven to the saturation point using square wave pulses and the external magnetic field is connected with an extra coil bending the hysteresis curve. When sensing current, the coil to bend the hysteresis curve can have only one round, e.g. it is threaded through a high permeability toroid. The output signal is the combined result of the two coils, often measured with a third coil, giving pulses accordingly to the external magnetic field. Figure 6 shows the current output without external magnetic field and Figure 7 shows the resulting output in case of existing external magnetic field with DC element. A precision flux gate sensor is presented in Figure 8. The pulses of the output signal can be rounded to the sine wave with capacitors and the normal negative feedback loop can be implemented with fourth coil to improve accuracy. Flux gate sensors are often very accurate and sensitive compared to Hall sensors or current transformers. [23]

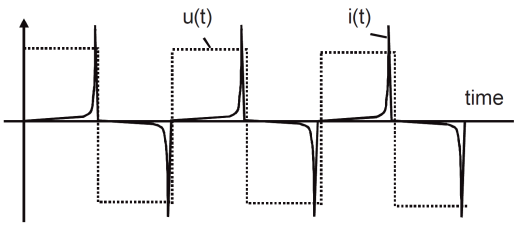

Figure 6. U(t) is the pulse used to drive the square wave pulses to the system and I(t) is the current output symmetric over the time axle.

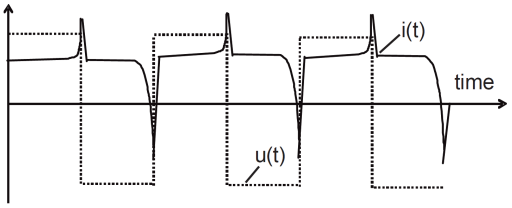

Figure 7. U(t) is the pulse used to drive the square wave pulses to the system and I(t) is the current output with DC-element over the time axle.

Figure 8. A precision flux gate sensor and logic.

2.2.5. Magnetoresistive Sensors

Magnetoresistance is a property of a resistor to change the value of its electrical resistance when an external magnetic field is applied to it. It was discovered by William Thomson (later Lord Kelvin) in 1857. He used pieces of iron and nickel as test subjects in magnetic field and found anisotropic magnetoresistance (AMR) [24]. Other types of magnetoresistance include for example giant (GMR) and colossal (CMR) magnetoresistances and superconducting quantum interference device (SQUID).

Potter stated in his article about anisotropic magnetoresistance: "At room temperature, the anisotropic resistance in alloys of Ni-Fe and Ni-Co can be greater than 5%. The theoretical basis takes into account spin orbit coupling and d band splitting. Other properties such as permeability, magnetostriction, and Hall voltage, have no simple relationship to magneto-resistance. Anisotropic magneto-resistance has an important use as a magnetic-field detector for digital recording and magnetic bubbles." [25]

Giant magneto-resistance can be achieved for example using magnetic and nonmagnetic layers. It can be significant in room temperature and grow when cooled [26].

Reig in turn stated: "Behind the utilization of GMR structures as read heads for massive storage magnetic hard disks, important applications as solid state magnetic sensors have emerged. Low cost, compatibility with standard CMOS technologies and high sensitivity are common advantages of these sensors. This way, they have been successfully applied in a lot different environments. In this work, we are trying to collect the Spanish contributions to the progress of the research related to the GMR based sensors covering, among other subjects, the applications, the sensor design, the modeling and the electronic interfaces, focusing on electrical current sensing applications." [27]

According to Ramirez, CMR is magnetoresistance associated with a ferromagnetic to paramagnetic phase transition where the material displays a transition from a high temperature paramagnetic insulator to a low temperature ferromagnetic metal. Near the phase transition temperature, which can exceed room temperature in some compositions, large magnetoresistance is observed and its possible application in magnetic recording has revived interest in these materials. [28]

SQUID requires typically very low temperatures thus it is not suitable for consumer electronics. Lee for example had a functional device on 77°K [29].

2.3. WSN's for Collecting Load Measurements

In the past few years wireless sensor networks (WSN) have become popular in energy monitoring systems. The key advantage of WSN's is that they do not require any new wires for communications, which may be difficult and expensive to install afterwards.

2.3.1. Wireless Sensors

Typically, a wireless sensor has not only a sensing component, but also on-board processing, communication, and storage capabilities. A sensor node is often responsible for data collection, in-network analysis, correlation, and fusion of its own sensor data and data from other sensor nodes. When many sensors cooperatively monitor large physical environments, they form a WSN. Sensor nodes communicate not only with each other but also with an edge router, sometimes also called as base station (BS), using their radios and disseminating their sensor data to remote processing, visualization, analysis, and storage systems. [30]

The capabilities of sensor nodes in a WSN can vary from simple sensor nodes monitoring a single physical phenomenon, to complex devices combining many different sensing techniques (e.g. acoustic, optical, magnetic). They can also differ in their communication capabilities, for example, using ultrasound, infrared, or radio frequency technologies with varying data rates, protocols and latencies. While simple sensors may only collect and communicate information about the observed environment, devices with large processing, energy, and storage capacities may also perform extensive processing and aggregation functions. Such devices often assume additional responsibilities in a WSN, for example, they may form communication backbones that can be used by other resource-constrained sensor devices to reach the BS. Finally, some devices may have access to additional supporting technologies, for example, Global

Positioning System (GPS) receivers, allowing them to accurately determine their position. [30]

2.3.2. WSN Architecture

A WSN typically comprises wireless sensors grouped in so-called sensor fields and communication infrastructure transmitting the sensor data to the centralized servers that store and process the sensor data for different applications. Figure 9 shows an example architecture of a WSN with two sensor fields, which comprises of four functional building blocks:

1. Sensors in multiple sensor networks measure their environment and transmit the data wirelessly to the edge routers using multi hop topology. Sensors may move from a sensor field to another, if they are all using the same protocol stack and have automatic discovery procedures. [30]
2. Edge routers forward the data of a sensor field to the internet.
3. Internet is used to transmit the data to the server.
4. Central server processes, analyses, stores, and mines the data.

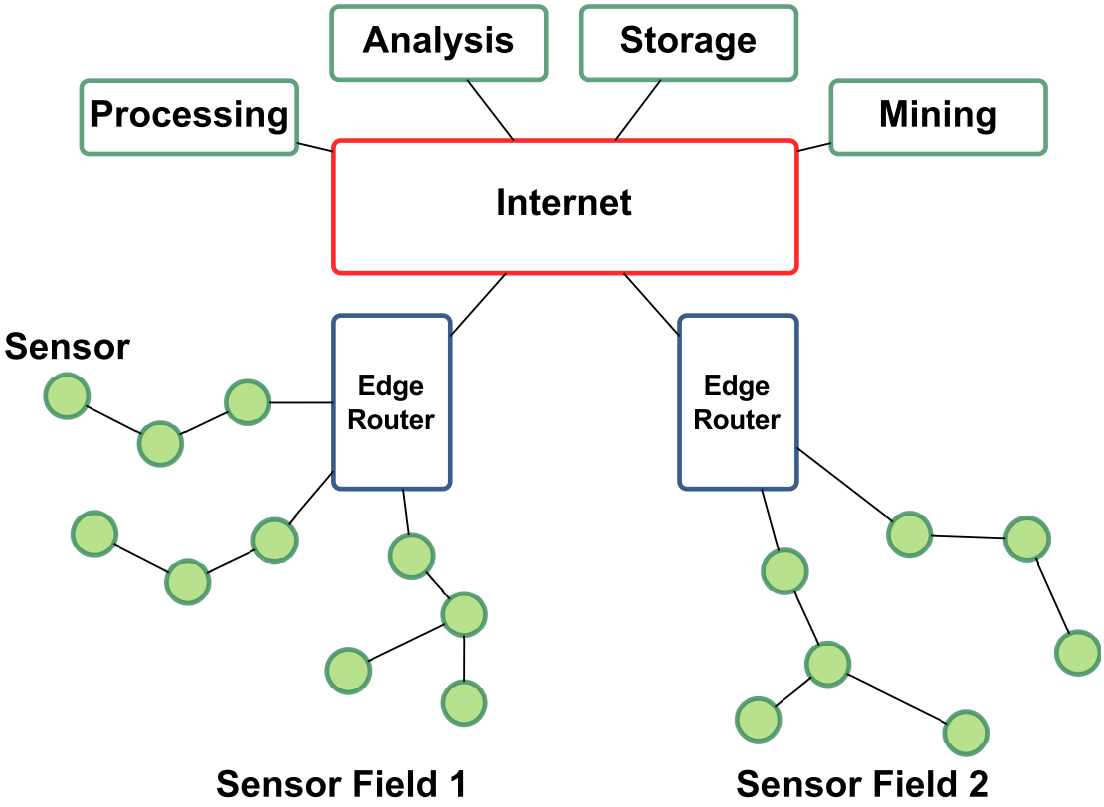

Figure 9. An example system architecture of WSN.

Figure 10 shows three possible IEEE 802.15.4 network topologies of a WSN sensor field: star, cluster tree and mesh. The star architecture results from the single hop network topology, where all devices connect directly to the edge router. The cluster tree can be formed if sensors can forward the data of other sensors to the edge router. In the mesh topology sensors are capable of connecting to each other. The redundant connections improve the reliability of the network as most sensors have multiple paths to the edge router.

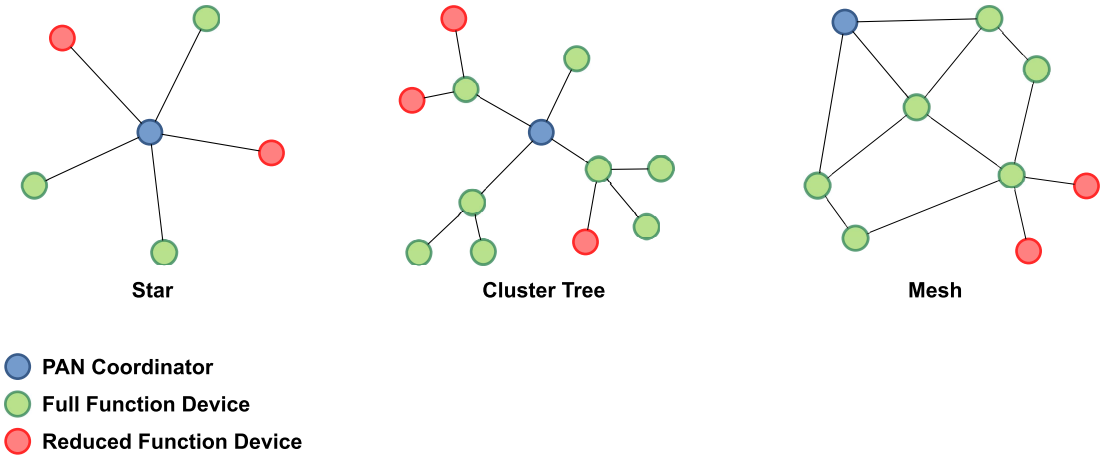

Figure 10. Examples of network topologies of WSN.

2.3.3. Protocol Stack

Figure 11 shows two protocols stacks commonly used in WSN's, ZigBee and 6LoWPAN. Both ZigBee and 6LoWPAN protol stacks use the IEEE 802.15.4 technology for wireless communication. The physical layer functions locally on 868 – 928MHz or globally 2400 – 2480 MHz band with BPSK, ASK or O-QPSK modulations resulting to 20 – 250 kpbs Bit rate. The Mac layer is responsible for connecting the node to WSN either with CSMA/CA, a beaconless system to share a transmission channel by sending reservation signal to unused channel before the actual data transmission, or with CSMA/TDMA, in which the PAN coordinator additionally determines beacon intervals accordingly to the busyness of a channel and beacons mark frame sizes to the data transmission called superframes. [31]

The ZigBee protocol stack over the IEEE 802.15.4 radio allows 64000 nodes per master and 128 bit AES encryption. The devices recognize profiles over the application framework, such as "Building Automation", "Remote control" and "Smart energy". [9]

The 6LoWPAN protocol stack has been developed to provide IPv6 addressing and routing for IEEE 802.15.4 nodes even not being actually tied to only those [32][33][34]. 6LoWPAN supports only IPv6 and UDP, whose headers are compressed to minimize header overhead in communication over lossy and low power IEEE 802.15.4 wireless links. [30, 6]

A particular application layer protocol of interest is CoAP which is specifically designed for constrained nodes and networks such as sensors implemented with 8-

bit microcontrollers and communicating over IEEE 802.15.4 links. CoAP has been developed by the IETF CoRE (Constrained RESTful Environments) working group, which aims at realizing the REST (Representational State Transfer) architecture for constrained nodes and networks in machine-to-machine (M2M) applications such as smart grids and building automation.

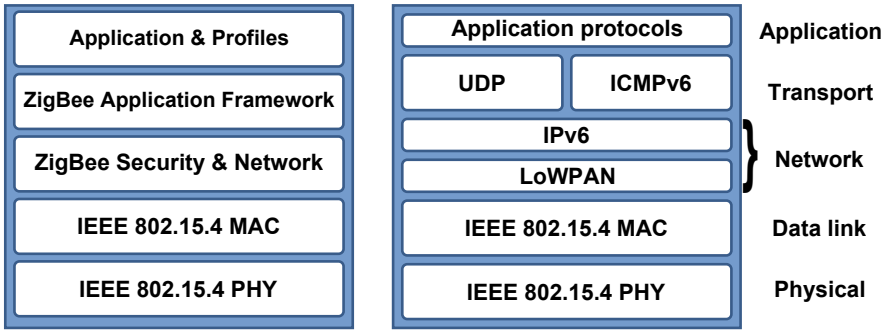

Figure 11. An example of WSN protocol stacks.

2.4. Examples

Two systems for monitoring energy consumption in a household with wireless sensor networks are presented as examples. Plugwise is a commercial system collecting detailed measurements of selected individual appliances with the ZigBee protocol stack. UBI-AMI version 1 is a research prototype developed at the University of Oulu that collects data on both the aggregate load and appliance level loads using the 6LoWPAN protocol stack.

2.4.1. Plugwise

A Plugwise system consists of a Circle+, one or more Circles, the Plugwise Stick and the Source software (Figure 12) [35]. The components communicate with each other wirelessly using the ZigBee protocol.

The Plugwise system has been designed to do three things:

1. Provide detailed information of energy consumption per appliance.

   A Circle contains a small power meter that registers energy consumption of connected appliances.

2. Save energy by creating switching schemes.

   The Source software allows creating switching schemes for appliances connected to the Circles. Thus, energy can be saved by switching off appliances in periods when they are not used. An appliance that has been switched off by a Circle can be turned on by simply removing it from the socket and putting it back on (or switched on and off at the socket). The switching scheme will resume from the next scheduled event.

3. Create virtual power groups and switch them wirelessly.

   The Source software allows grouping Circles into virtual power groups e.g. according to rooms and switching them wirelessly .

Figure 12. An example of the Plugwise system. From top to down: UI of Source, 8 Circles and Circle+, Stick.

The Plugwise system is based on a wireless mesh network created with the ZigBee protocol on the 2.4 GHz band. The network uses 128-bit AES encryption to protect the energy consumption data and to guarantee the privacy of the user. The mesh network self-organizes itself so that new Plugwise modules are discovered and joined in the mesh automatically. Each Plugwise module is identified by its own unique code and their firmware can be upgraded over the air via the Source.

The Plugwise Stick attached to the USB port of a computer connects the Plugwise mesh network to the computer (and to the Internet) and to the Source software. The network is coordinated by one Circle+ that keeps track of the Circles in the network. Circle+ has a real-time clock and a battery and it periodically synchronizes time with the Circles. A Circle measures the energy consumption of the appliances plugged to it, stores the power consumption data and transmits it to the Stick. A Circle is also equipped with a standby killer, which entirely interrupts power to a connected appliance when it switches to the standby mode, to prevent unwanted energy usage.

The Source software is the "brain" of the Plugwise system. It controls the Plugwise system and provides detailed information of the energy consumption in form of overviews, diagrams, and totals over time as cost, energy and cost savings. The Source allows switching appliances connected to Circles on and off, and implementing switching schemes for individual Circles and their groups.

The Plugwise system includes also other components:

- "Stealth" is a built-in module for measuring and switching in situations where it is undesirable or impossible to use a Circle. Stealth is similar to Circle in terms of its functionality.

- "Switch" The Plugwise Switch is a wireless switch for creating tailored groupings of Circles and Stealths.
- "Strong 604" is a main electricity meter and sub meter that measures the total energy consumption of a complete electric installation.
- "Strong 103" is an electricity sub meter that measures the total energy consumption of a group or department within a complete installation.
- Other devices include touchscreen control panel, sensors for humidity and temperature, light and motion detector and a device for remote access.

2.4.2. UBI-AMI version 1

UBI-AMI is a research prototype developed at the University of Oulu for real-time metering of aggregate power consumption and appliance level loads in homes with wireless sensors. [7]

Architecture

Figure 13 shows the architecture of the UBI-AMI system, which comprises of three functional building blocks:

1. Sensors in multiple 6LoWPAN sensor networks measure the loads, illumination and temperature. Each network has a router collecting packets from multiple sensors.
2. Central UBI-AMI server receives packets from the routers, stores the data in a database and creates different representations of the data.
3. User can browse the measurement data with a web browser and subscribe to RSS feeds summarizing the data. Further, the user can control the sensors and subscribe to email/SMS alerts based on load measurements.

Wireless Sensors

The UBI-AMI system involves two types of wireless sensors, the mains sensor and the socket sensor. Both sensors are furnished with a Radiocrafts RC2301 radio module which is equipped with an IEEE 802.15.4 radio on the 2.4 GHz band [36]. The radio module is flashed with the Sensinode NanoStack 2.0 protocol stack, which implements the IETF 6LoWPAN specification for transmitting IPv6 packets over IEEE 802.15.4 devices [37, 38]. Effectively, the protocol stack provides the sensors with half-duplex multi-hop IPv6 connectivity.

A socket sensor (Figure 14) measures the loads of individual devices or groups of devices equipped with pluggable power cords. The socket sensor is furnished with a 1.5 m three-socket extension cord, to allow easy placement of the sensor unit and the load measurement of multiple appliances. A relay capable of switching 16 amperes is integrated to turn on/off the appliances plugged into the sensor.

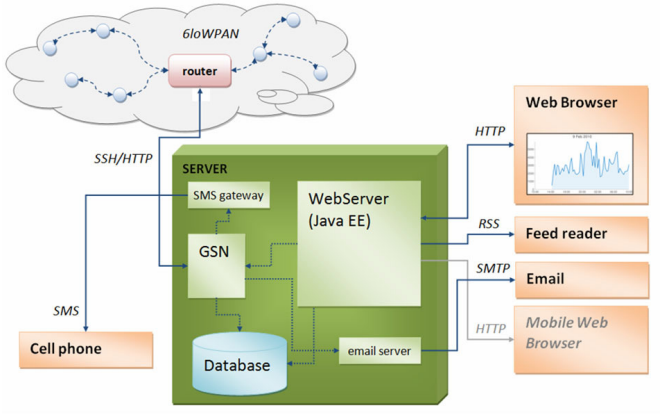

Figure 13. The architecture of the UBI-AMI system.

A mains sensor (Figure 15) measures the load at the root of the load tree of a building, including all non-pluggable devices such as electrical heating, hot water boiler and lighting with a simple phototransistor counting the pulses of the optical test output interface of a main switch board.

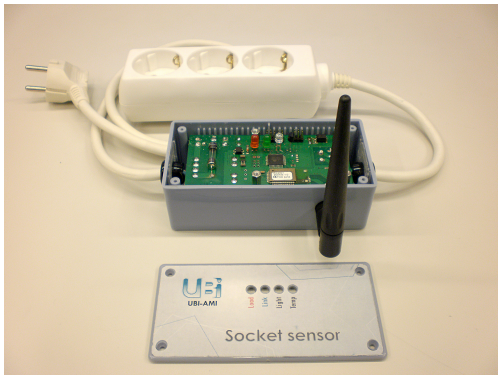

Figure 14. The socket sensor of the UBI-AMI version 1.

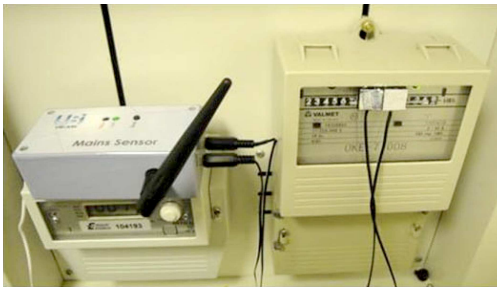

Figure 15. The mains sensor of the UBI-AMI version 1. Below the sensor box is the optical pulse input.

WSN Router

The WSN router was implemented from an affordable Linksys WRT54GS WLAN router by adding a Radiocrafts RC2301 radio module to a free serial port connected to an external antenna connector (Figure 16) [39]. The Linksys router was flashed with a customized Kamikaze OpenWRT Linux firmware capable of routing packets between the 6LoWPAN network and the Internet [40]. When connected to any IPv4 network providing an IP address via DHCP, the router establishes two SSH connections to the UBI-AMI server. The first connection is used to securely transfer the packets received from the sensors using the HTTP protocol, together with any commands between the router and the server. The second connection is used to access the router remotely for management purposes. The wireless links between the router and the sensors are protected by 128-bit AES encryption.

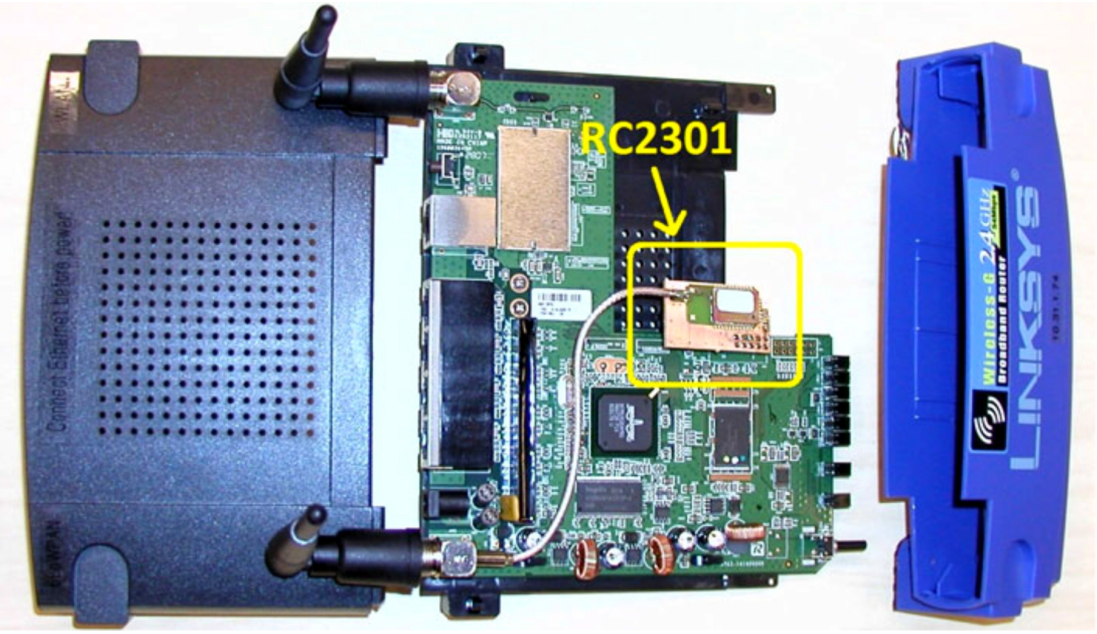

Figure 16. WSN router with the placement of the RC2301 radio module highlighted.

Server

The UBI-AMI server was realized in Java atop the open source GSN (Global Sensor Network) middleware in [41]. So-called wrapper components receive the measurement data from the routers and store the data into a MySQL database [42]. For security purposes the server authenticates each router with MAC address filtering and all communication takes place through SSH tunnels.

User Interface

The user interface was implemented as a website atop the open source GlassFish application server as Java Server Pages [43]. Figures 17 and 18 shows screenshots of the two most commonly used pages, power and energy. Other views based on the sensor data include energy bill, temperature, and illumination. Each type of data can be viewed on different time scales. The UI has separate tabs for drawing the floor plan and for configuring alarms received either via email or SMS to mobile phone. After giving the friendly names (e.g. 'TV' or 'fridge') to the sensors, they can be viewed and switched on/off by clicking the icon.

The UI has also a separate tab for configuring settings such as the price of energy and RSS feeds reporting the real-time power consumption for the last 1, 4 or 24 hours. The header shows the user's current real-time energy consumption with relative change over the past 24 hours.

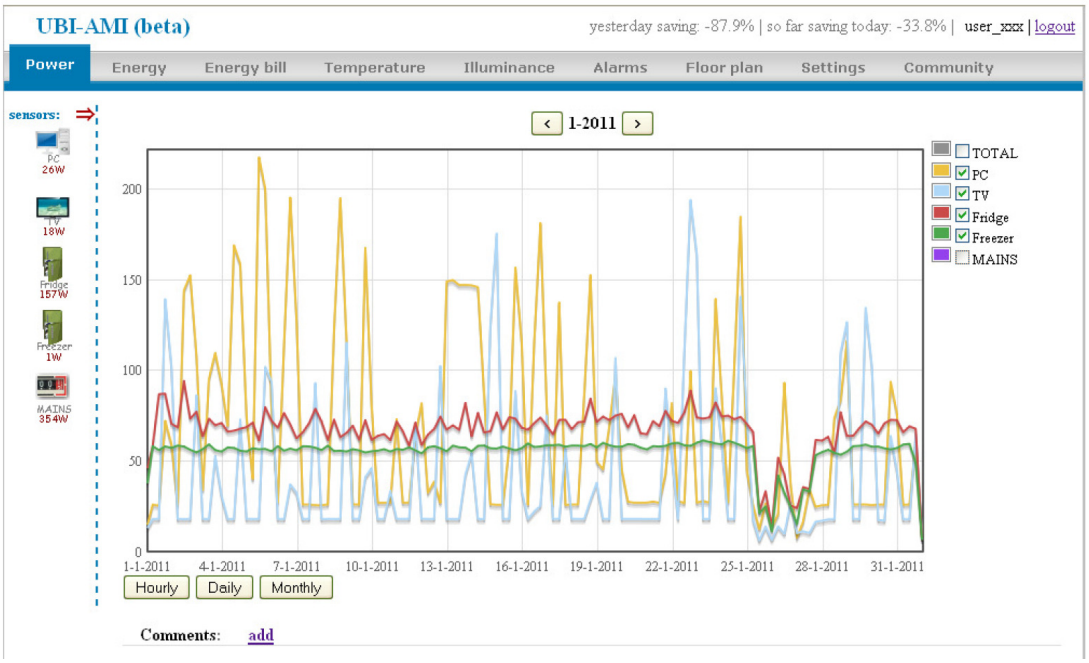

Figure 17. A screenshot of the power consumption display of UBI-AMI user interface.

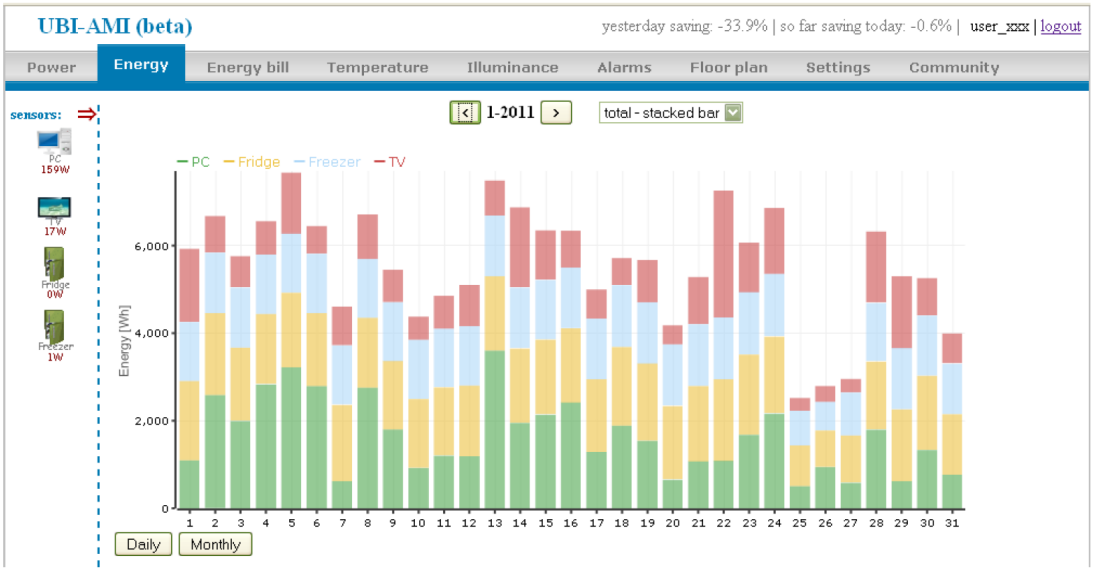

Figure 18. A screenshot of the energy display of UBI-AMI user interface.

Field Evaluation

The UBI-AMI system was evaluated via an 11-month field trial at seven households in the Oulu region in 2010. Each household was provided with a demo kit comprising of a router, a mains sensor and four socket sensors. All seven households lived in a detached house equipped with electrical heating, an electric sauna and a hot water

boiler. Quantitative data was obtained by logging at the server and qualitative data by opening and follow-up interviews and questionnaire studies of the test users.

In the opening interviews the test users listed easy deployment, low operational expenses, possibility to measure electricity consumption of an individual appliance and timeliness of the electricity consumption data as the most relevant features of the UBI-AMI service. While all test users expected the UBI-AMI service have some sort of an effect, none expected the electricity consumption to reduce a lot.

According to the server logs the daily power and energy views dominated the usage of the interface as expected. Exactly one test user reported the system to have had reduced the energy consumption in their household. The main technical difficulty experienced by the test users was the loss of data, which could be attributed to intermittent Internet connection of the router and the unreliability of the UDP protocol used by sensors to transmit the data. Further, the low-power 2.4 GHz wireless links were found to have limited range and poor penetration in brick buildings.

The test users reported that their continuous interest in real-time loads of individual appliances wore out rather quickly. Instead, they would have preferred visualizing the monetary expenses of energy consumption, together with any rapid relative changes, as an ambient media whose observation would not require any conscious or dedicated action on their part. Further, sensors for measuring non-socket appliances such as sauna stoves and hot water boilers were requested, together with automatic incorporation of outdoor temperature, which in Finland is crucial for assessing the contribution of electric heating into the power consumption.

3. DESIGN

This Chapter reports the design of the Mains sensor for the UBI-AMI version 2 that is partly pre-determined by the design of the Mains sensor of the UBI-AMI version 1.

3.1. Requirements

The following requirements were partly elicited from the findings of the field evaluation of the UBI-AMI version 1 and partly set by the UBI-AMI project.

3.1.1. Functional Requirements

The Mains sensor must be able to measure both the total energy consumption of a household and the loads of individual integrated elements such as sauna, stove, floor heating and hot water boiler from the electric board.

3.1.2. Performance Requirements

1. The accuracy of the measurement of the total energy consumption must comply with standard EN50470-1:2006 [44]. Further, the value of total consumption must equal the reading of the kilowatt hour meter of the household, to avoid providing conflicting information for the consumer.
2. In the measurement of the energy consumption of integrated elements, the Mains sensor must be able to recognize at minimum a change of 1 A in current if an integrated element is switched off or on [44].

3.1.3. External Interfaces

1. The measurement of the total load conducted using the kilowatt hour meter's test pulse output must be comparable to the kilowatt hour meter's reading even if some of the data would be lost during transmission. Therefore, the data of pulse input must be handled similarly to the standard IEC62052-11:2006 [45]. It states that the pulse frequency of a test output of a kilowatt hour meter must result at least 1/10 of the accuracy requirement of the meter's standardization class, but still not go higher than 2.5 kHz. The capacity of the energy meter should be at least 1500 hours at full power. This means that using the Mains sensor with the maximum of 35 A main fuses, the maximum number of pulses to be recorded is:

$$3 * 35A * 230V * 10000pulses/kWh * 1500h = 362,250,000pulses \quad (10)$$

The pulse can be modulated. In the case of optical output, the wavelength of the light pulse must be from 550 nm to 1000 nm and the strength measured from 9

- 11 mm of the meter's surface must be from 50 µW/m^{2}to 1000 µW/m^{2}during the pulse and 2 µW/m^{2}maximum otherwise. If a galvanic connection of the test output is used, the operating voltage must be fed from the external device to the test output. The pulse can be less than one volt when it is on and up to 27 volts when it is off. The maximum current is 27 mA. The output pulse waveform is presented in Figure 19. For the galvanic test connection it is minimum of 30 ms on and respectively minimum of 30 ms off. Rising and falling times are maximum of 5 ms from 10 % to 90 %. The waveform must not be homogenous. [46]

2. The loads of integrated elements connected as groups must be measured from individual fuses of the fuse board. The Mains sensor must be able to measure at minimum 30 circuit breakers so that the measurement heads use only safe voltage levels.

3. It must be possible to program the MCU of the Mains sensor multiple times during prototyping. The programming interface must be chosen according to the MCU.

4. A wired or wireless debugging interface must be provided as it is essential for protocol level and application level debugging and testing.

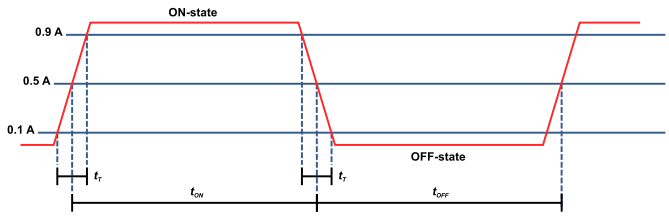

Figure 19. The example of the required waveform for the test output of the kilowatt-hour meter. Minimum on/off duration is 30 ms and maximum rise time (t_T) is 5 ms. i = maximum voltage of the pulse.

Design constrains

1. The wireless radio module to be used in the Mains sensor is Radiocrafts RC1180 868 MHz - 870 MHz module equipped with the Sensinode Nanostack 2.0 closed software [47, 38]. The specification of the NAP interface of the software is provided by our research partner Sensinode.

2. The measurement heads for the circuit breakers must be of low cost type, to keep the total unit price of the Mains sensor reasonable for domestic customers.

3.2. Technology Choises

Particular components were given such as the wireless radio module. Further, the optical output of the kilowatt hour meter was to be measured by the same phototransistor

and input circuitry that was used in version 1. The measurement of the galvanic output is straightforward, requiring a connection through an optocoupler to ensure safety. This leaves the measurement of circuit breakers and the selection of the processor as the important technology choices.

3.2.1. Measurement of Circuit Breakers

Important properties of different candidate methods for measuring the loads of the circuit breakers are presented in Table 1. A method is considered to be intrusive if the current must permanently run through the measurement device. Accuracy is considered sufficient if 1 A current can be detected. Safety is considered to be reached if a galvanic connection is not mandatory in the measurement. Size is small enough if sensors fit inside the circuit breaker board acquired for testing. The two least expensive methods are considered to be economically viable. In conclusion, Hall sensor without feedback loop is considered as the most suitable technology for measuring the loads of circuit breakers.

Table 1. Comparison of methods to measure current (x = suitable, o = not suitable):

Method	Intrusiveness	Accuracy	Safety	Size	Price
Shunt Resistor	o	x	o	x	x
Hall sensor	x	x	x	x	x
Hall sensor, feedback	x	x	x	x	o
Current transformer	x	x	x	o	o
Current transformer, feedback	x	x	x	o	o
Fluxgate sensor	x	x	x	o	o
Magnetoresistive sensor	x	x	x	x	o

3.2.2. Processor

Atmel's 8-bit microcontroller ATmega2560 is chosen for its high compatibility with the existing source code made for the ATmega164 in the UBI-AMI version 1 [48]. With proper libraries the MCU is able to handle the 32-bit numeric range required for counting pulses. The MCU can use 5 V Vcc so it is capable of powering up the Hall sensors that need a minimum of 4.5 V. Thus, a separate "Enable" signal is not needed, but the Hall sensors can be just powered on and off.

The MCU has a hundred pins including four universal synchronous/asynchronous receiver-transmitter (USART) serial ports, 10-bit ADC with the total of 2 LSB accuracy with internal sample and hold circuitry and possibility to connect two I/O's to the same low active interrupt that can be used as lines for pulse inputs. After using two serial ports the MCU still has enough free GPIO's to connect both power and GND for 30 Hall sensors, which ensures that the signals of different sensors do not interfere with each other.

The MCU has 4 Kbytes of EEPROM (Electronically Erasable Programmable Read-Only Memory) for storing the data and some calibration values during a possible power outage and a JTAG (Joint Test Action Group) interface for programming and debugging.

3.3. Architectural Design

3.3.1. UBI-AMI version 2

Figure 20 shows the overall architecture of the UBI-AMI version 2 system, which comprises of three functional building blocks:

1. Wireless sensors in multiple 6LoWPAN sensor networks measure the loads and turn on/off devices connected to the sensors. Each network is connected to an edge router collecting packets from multiple sensors over a multi-hop mesh topology, i.e. a sensor is able to forward packets of other sensors. The edge router forwards packets to the UBI-AMI server over Internet.

2. The central UBI-AMI server comprises of a resource directory, a proxy for coordinating communication with clients, a database for storing the sensor data, and a web server for creating different representations for user interface.

3. User can view the measurement data and control the sensors with a web browser on a PC or on a smart phone that communicates with the web server in the UBI-AMI server through Internet.

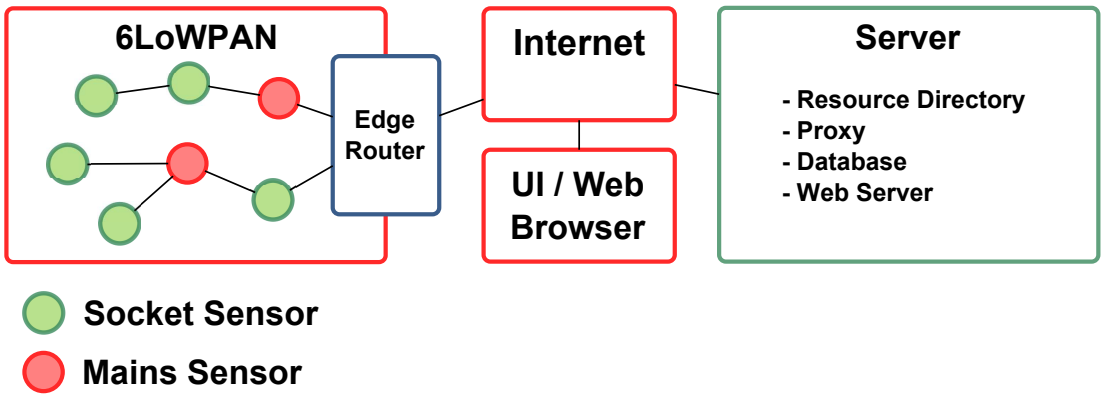

Figure 20. Architecture of UBI-AMI version 2.

Figure 21 illustrates the role of the so-called reverse proxy [49] in mediating the communication between the clients using the HTTP protocol and the components using the CoAP protocol. The sensors act as servers having resources, for example the measurement data, and register themselves to the resource directory (RD). The proxy obtains a list of sensors from the resource directory and makes it available to the clients. A

client requests the sensor data from the proxy which in turn obtains the data from the sensors and forwards it to the client.

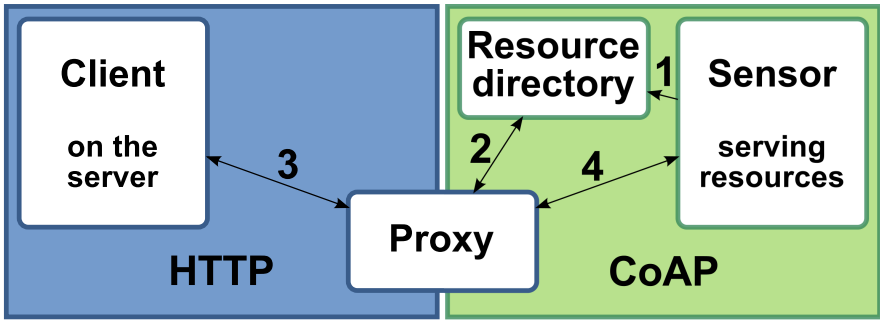

Figure 21. The proxy mediates communication between HTTP nodes and constrained CoAP nodes.

3.3.2. Mains Sensor Hardware

The overall hardware architecture of the Mains sensor is illustrated in Figure 22. The optical and galvanic pulse outputs of the kilowatt hour meter have their separate inputs, equipped respectively with an amplifier and an attenuator to bias the signal to the desired dynamic range and an optocoupler to isolate hazardous voltages in normal or unpredicted situations. The Hall sensors measuring the loads of circuit breakers are connected directly to the MCU through dedicated input lines since the MCU is able to power up the Hall sensors and the MCU has enough GPIO's for 30 Hall sensors. The ADC is done by the MCU.

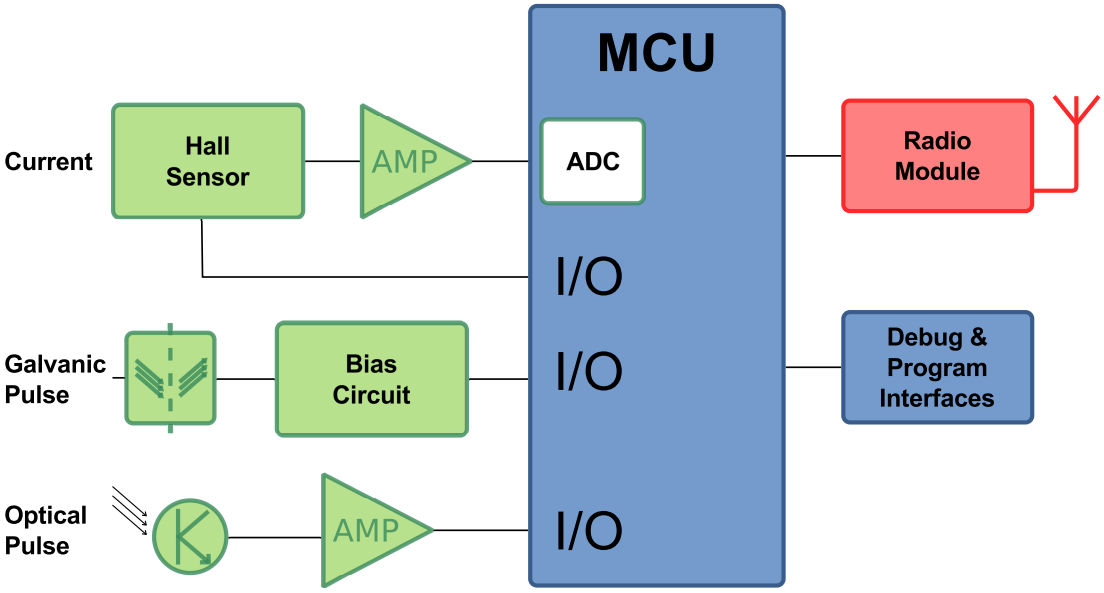

Figure 22. A block diagram of a sensor HW.

3.3.3. Mains Sensor Software

The state machine implemented by the software of the Mains sensor is presented in Figure 23. Once the HW and SW are initialized and the connections are set upon startup, the SW implements the following the main loop where time critical parts are triggered by interrupts:

1. Refresh the RD (triggered by interrupt)
2. Read measurements if semaphore is on (triggered by interrupt)
3. Execute continuation code (if continuation code received in a message)
4. Parse message (if there are incoming NAP messages)
5. Parse and send message if semaphore is on (if measurement is requested and measurement is ready)
6. Send message of a new resource to the RD (if continuation is ready)
7. 100 ms delay

The asynchronous timing of received messages and the unpredictability of the use of processing resources requires using as little as possible time critical processing. Therefore, even when the reading of the measurements would ideally be located in the interrupt service routine (ISR), it is designed to use only interrupt driven semaphore for not to reserve too much of processing time in the ISR and potentially block other functions.

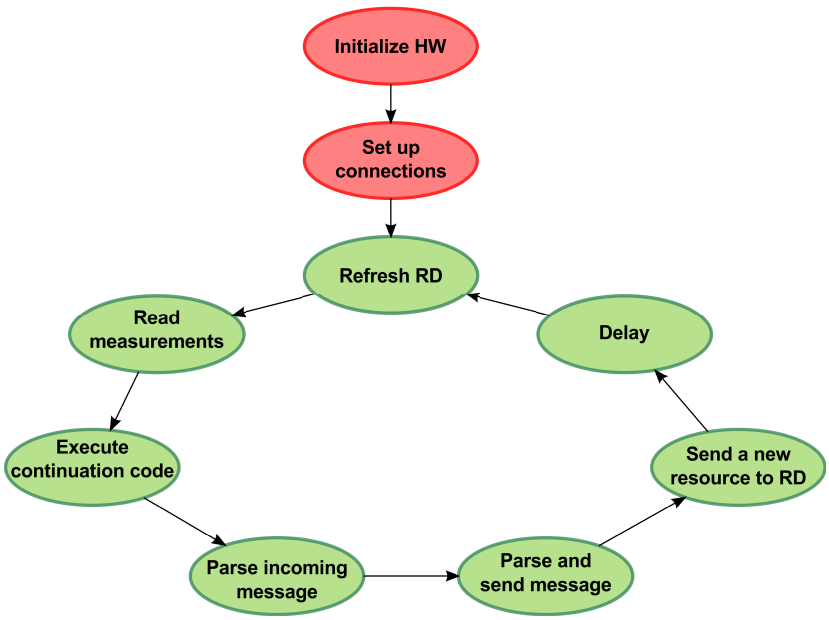

Figure 23. The figure presents a state machine of Mains sensor. Initializations are in red bubbles on top of the image, and main loop is presented with green bubbles.

4. IMPLEMENTATION

4.1. Hardware

The circuits were simulated with the LT-Spice simulator and the essential parts of the circuits were prototyped and measured before integration into the PCB.

4.1.1. Pulse Inputs

The optical and galvanic inputs of the kilowatt hour meter's test output can be connected to the same interrupt vector using either the same or possibly two different pins of the MCU. They both only need appropriate circuitry to input the pulse which triggers an interrupt.

Galvanic Pulse Input

Figure 24 shows the schematic of the galvanic pulse input. It is isolated from the microcontroller with a photocoupler to ensure the safety of the MCU with different test outputs [50]. A trimmer potentiometer is used as a dropping resistor for the input diode of the optocoupler. MPULSE+ and MPULSE− are connected to the kilowatt hour meter. ISOL_PULSE is connected to the microcontroller.

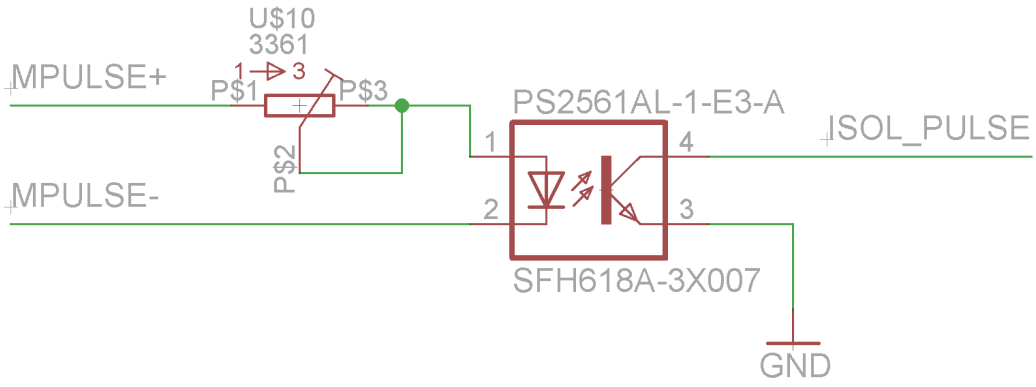

Figure 24. The schematic of galvanic pulse input. The dropping resistor is on the left and the photocoupler on the right. The "ISOL_PULSE" is connected to the microcontroller.

The properties of the dropping resistor can be calculated knowing the properties of the diode and possible input voltages of the circuitry. The input diode has 1.2 V threshold voltage with 10 mA current. The dropping resistor must be able to drop

voltage from 27 V to 1.2 V, i.e. 25.8 V with 10 mA. The maximum resistor value needed is found using the equation (1) that gives the voltage over a resistor:

$$U = RI <=> R = \frac{U}{I} \tag{1}$$
$$R = \frac{25.8V}{10mA} = 2580\Omega,$$

where

U = voltage,
R = resistivity,
I = current.

5 KΩ trimmer potentiometers are used since we had those readily available. Thus, the pulse input can be connected to anything between 1.2 V and 27 V with a fair safety margin.

There should be extra pins on the layout close to the input circuitry to provide external operating voltage and GND in case of open collector type test output signals of the kilowatt hour meter.

The signal out to the microcontroller is connected to the pin that can be pulled up with the internal pull-up resistor of the MCU. According to the datasheet this setup with interrupt signal being low active gives the highest possible maximum frequency over 20 KHz to the photocoupler. This is adequate since the maximum frequency of the test output is 2.5 KHz. The signal to the MCU can be considered digital.

Optical Pulse Input

Figure 25 shows the approximated simulation circuitry of the optical pulse input. The simulation results of the circuitry are shown in Figure 26. The frequency of the simulation is determined from an average household having 3*35 A main fuses and 10000 impulses/kWh type test output on the tariff meter which is common in the Oulu region and used by the utility company sponsoring the project. The frequency is calculated:

$$\frac{3 * 35A * 230V * 1h * 10000impulses/10^3Wh}{3600s} = 67.08Hz \approx 68Hz \tag{2}$$

The circuitry is very sensitive and only gives wider or narrower pulses according to the frequency. The rising and falling times are counted in the simulation according to the standard [45]. As seen in Figure 26, the signal to the MCU can be considered digital.

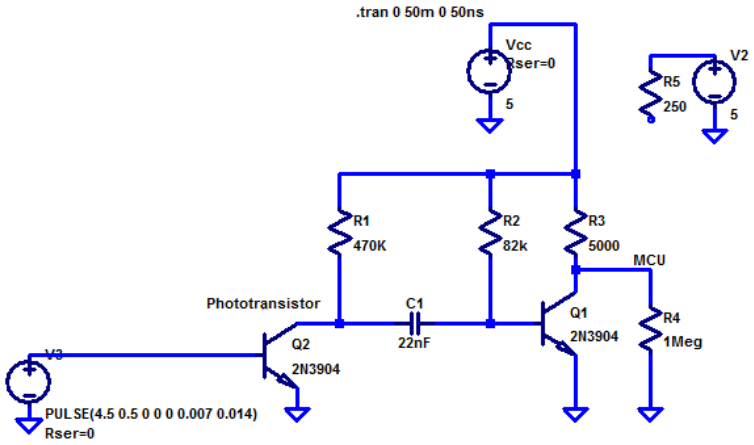

Figure 25. The schematic of the optical pulse input simulation circuitry. V3 is the light pulse, Q2 approximates the phototransistor, V2 and R5 are modelling MCU's pull-up resistor not connected, R4 is MCU's input resistance.

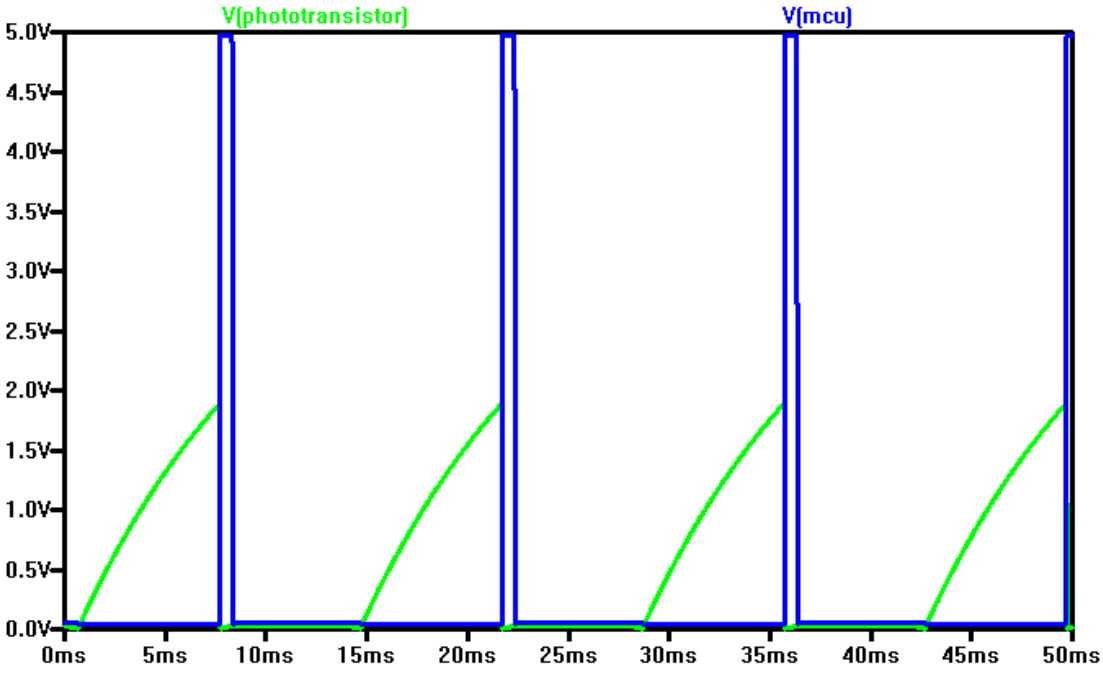

Figure 26. The results of the optical pulse input circuitry simulation of the maximum of the household of 68 pulses/second. The green line is the incoming signal from the phototransistor just before the capasitor C1. The blue line is the signal from the circuitry to the MCU.

The optical pulse input for the kilowatt hour meters test output is connected to the same interrupt vector as the galvanic one. This makes it possible to use the same

code for both inputs. The same input circuitry of the previous version is used with only one improvement: the pull-up resistor to feed the amplifier is replaced with a trimmer potentiometer. This gives the possibility to raise some possible disturbances above to the decision level of 30 % of the Vcc used by the MCU's input. To get the best possible signal the pull-up resistor should not be on, so it would be ideal to connect this circuitry to another physical pin of the MCU but still to the same interrupt vector with the galvanic input. The optical signal is collected with a Motorola MRD14B cascade phototransistor and a MMBT3904LT1G transistor is used to amplify the signal pulses [51, 52] (Figure 27). The amplifier transistor was originally drawn to be BC847, but the 2N3904 NPN transistor was used instead because it was readily available. Also, it is not a so critical part when the transistor is used as a switch.

Wavelengths over 800 nm should be collected with an infra-red (IR) phototransistor. The wide range of optical signals in kilowatt hour meters and any ambient lighting make it challenging to achieve accurate measurement. According to the local utility company even commercial professional equipment can have compromised accuracy. Thus, the optical pulse input is included in the PCB only for convenience. If more sophisticated optical inputs are required, they should be connected through the galvanic input with an external device.

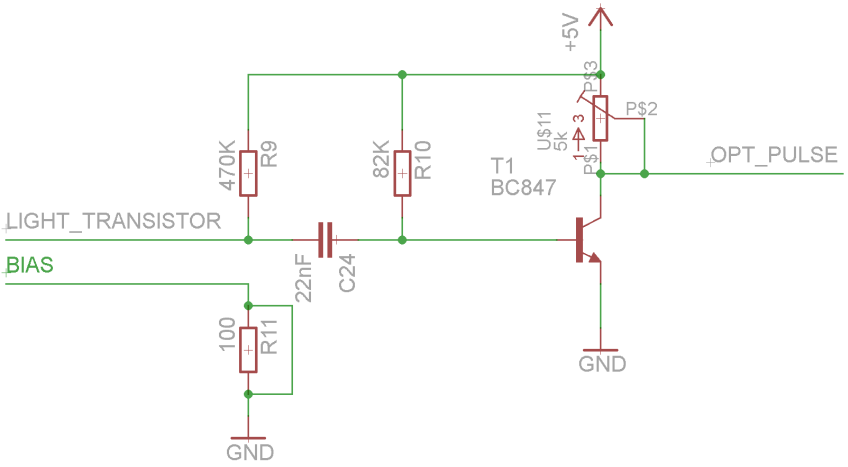

Figure 27. The schematic of the optical pulse input circuitry. The phototransistor is connected with a connector and extension wire to the lines on the left. R9 feeds the operating voltage to the light transistor,on the right is the line to the MCU.

4.1.2. Hall Sensor

Figure 28 shows the CSLT6B100 open loop Hall sensor that fulfills the requirements. It is a bipolar sensor giving voltage deviation from the middle of the supply voltage according to the measured current. The output stage of the Hall sensor is sink/source type. [53]

Figure 28. The Hall sensor is the smaller one on the left and the current transformer with the clamp is on the right.

The amplifier biasing the output of the Hall sensor into the desired dynamic range was designed according to the example circuits of the datasheets of Linear's LT1001 precision operational amplifier (OA) and to the "improved precision rectifier" and "simple AC meter" described in [54, 55] The dynamic range of the signal out from the amplifier circuit is designed to be sufficient for measuring currents between 0 A to 16 A. In that case the output signal from the amplifier to ADC is between GND and Vcc.

The first stage on the left of the simulation circuit shown in Figure 29 amplifies the dynamic range of the input signal from the Hall sensors to the maximum of the Vcc with the result of the measurement of 16 A through the sensor. The maximum output of Hall sensors is 18.5 mV/A yielding the maximum voltage of:

$$16A * 18.5mV/A = 296mV, \tag{3}$$

The OA's have their own Vcc from -9 V to 9 V, so the only restrictions between GND and Vcc follow from the abilities of the ADC. The typical Atmel ADC is rail to rail so the whole range between GND and Vcc is at our disposal except for a small safety margin. A Hall sensor having the same Vcc of 5 V as the MCU's output is able to give it without any constraints as well. Amplifying the maximum of 296 mV as near to the Vcc as possible gives the best possible resolution out of the ADC. The amplification of the first stage being non-inverting is calculated as:

$$\begin{aligned} V_out = V_in * (1 + \frac{R_f}{R_g}) = V_in * (1 + \frac{R_5}{R_4}) = 296mV * (1 + \frac{549k\Omega}{36.5k\Omega}) \\ = 4.748V \approx 4.75V, \end{aligned} \tag{4}$$

This gives room for possible errors at this point:

$$\frac{5V - 4.748V}{5V} * 100\% = 5.036\% \approx 5\%, \tag{5}$$

The signal input is connected via capacitor C1 in the simulation circuit accruing high pass (HP) effect to prevent any DC effect since only AC measurement is desirable. The DC level on the outputs of the Hall sensors is half of the Vcc and must be blocked. The amplifier has also capacitor C3 for one pole low pass (LP) filter to cancel thigh frequency noise. The frequency of the pole, i.e. the cutoff frequency, is calculated with the Formula (6) according to the first order RC filter:

$$f_c = \frac{1}{2 * \pi * R * C} = \frac{1}{2 * \pi * R_5 * C_3} = \frac{1}{2 * \pi * 549k\Omega * 470pF} \\ = 616.808Hz \approx 600Hz, \tag{6}$$

where

f_c = cutoff frequencyvoltage,
R = resistor value,
C = capacitor value.

The cutoff frequency is over ten times the 50 Hz AC frequency to be measured. Generally, f_c being over a decade away from the desired frequencie is not considered to influence to the results. The R_1 is simply a result of the simulation to fine tune out the small offset of the operation amplifier.

The next two stages are the "improved precision rectifier" and a peak value detector circuitry since the "simple AC meter" was not sufficiently accurate in the simulations and in the first prototype circuit. The capacitor C_2 takes the peak value that can be cleared with connection to the I/O-pin of the MCU that is modeled disconnected with a large resistor R_5 of 1000 MΩ. There is also a zener diode added on the output to the ADC as protection against temporary 9 V offset during the startup of the circuitry which was observed during prototyping.

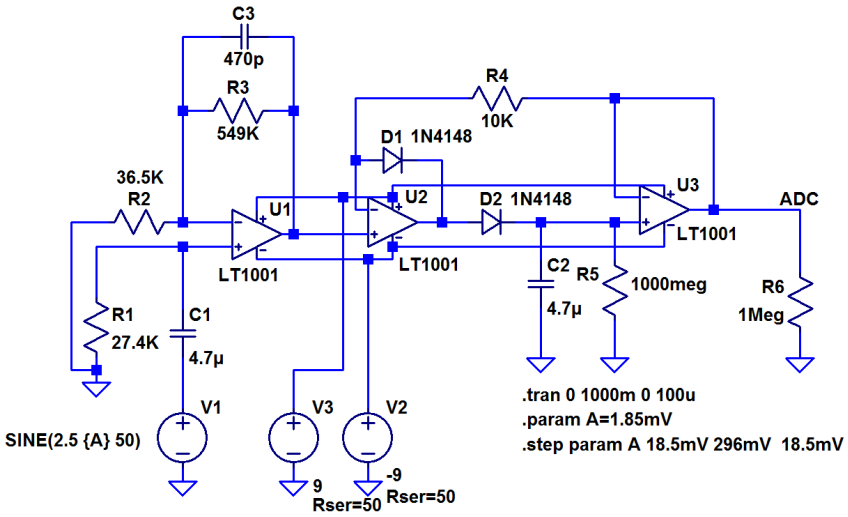

Figure 29. The schematic of the measurement amplifier for Hall sensors for simulations. The signal in is stepped modelling currents of 1 A to 16A.

The simulation results shown in Figure 30 support the calculations. The output of the amplifier settles as a straight line after 0.7 seconds. The highest possible value with 296 mV AC input is 4.72968 V due to the fine tuning of the circuitry with the offset resistor at the first stage and the feedback resistor over the latter two stages. The curves in the picture correspond to values measured from 1 A to 16 A in 1 A steps. The lowest value is 295.886 mV.

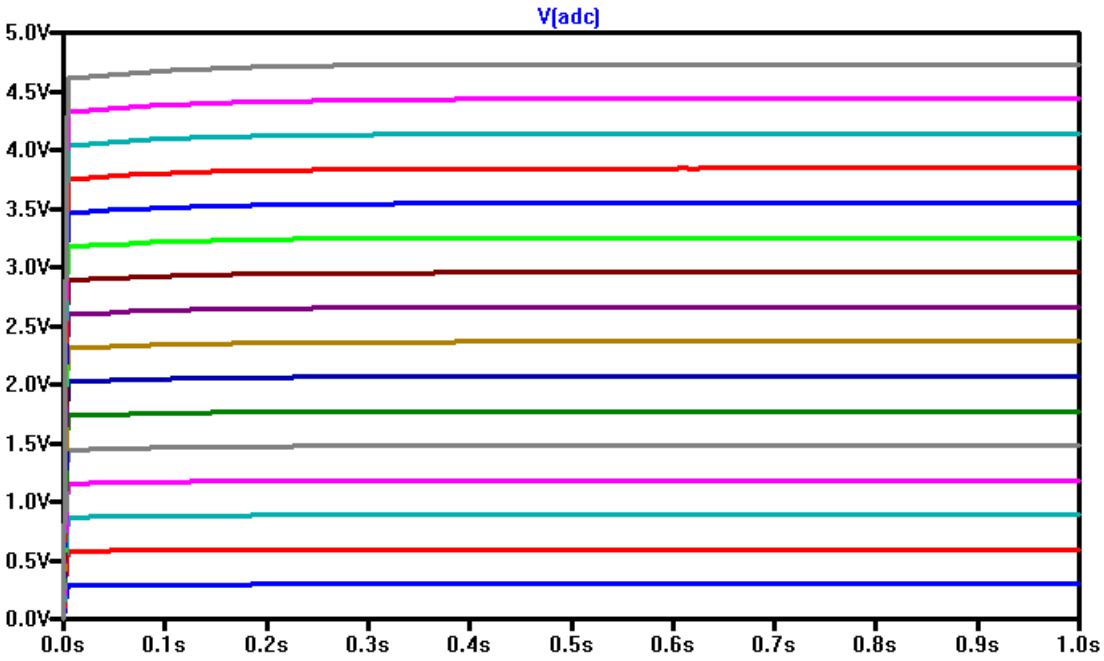

Figure 30. Output of the measurement amplifier to the MCU when feeded with 18,5 mV to 296 mV in regular steps of 18,5 mV.

4.1.3. Connections of the MCU

The connections to the MCU are presented in Figure 31. All Vcc inputs have a noise cancelling capacitor next to them. The Reset is pulled up with an external pull-up resistor although internal resistor could have been used as well. RXD and TXD are the USART-connections to the radio module. The crystal is connected to the XTAL1 and XTAL2 and capacitors are connected to the crystal as proposed in the datasheet. AREF1 and AVCC with capacitors and a coil are the reference voltage for the ADC and the components are for cancelling noise. ISOL_PULSE and OPT_PULSE are the pulse inputs. ADC is the input for the measurement amplifier of the Hall sensors. SAMPLE_OFF is to clear the sample and hold circuitry. JTAG connector is for programming and debugging. P_LED stands for power LED and it is connected to the red LED indicating the state of functionality so that the LED is on if power is on and there is no jam in the SW. I_LED stands for a green indicator LED that is used to indicate the activity of the radio link and for debugging purposes. The UART connector is for the asynchronous mode of the USART and it is used for debugging messages and for

a simple UI in calibration when connected to the serial port of a PC via an external USART-RS232 converter.

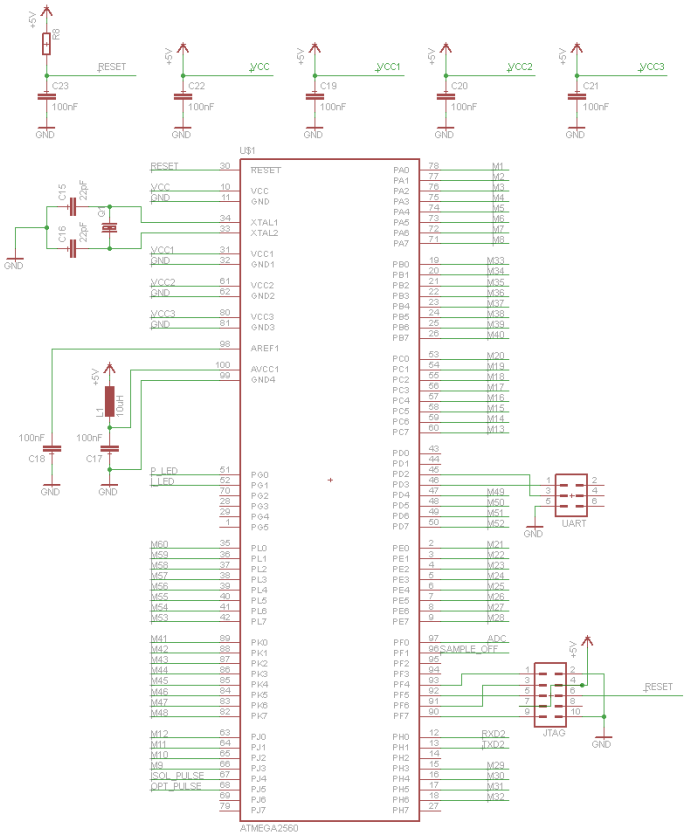

Figure 31. The schematic shows the connections of the Mains sensor's MCU. Vcc-pins have capasitors to the ground to cancel the noise and the reset has a pull-up resistor.

4.1.4. Connections of the Radio Module

The connections of the radio module are shown in Figure 32. They follow the original design of the Radiocrafts datasheet unless recommended otherwise by Sensinode. The Vcc of the radio module is lower than elsewhere in the circuitry. It is fed through ferrite bed and a capacitor is used next to VCC13 pin to cancel the noise. The antenna is connected to the RF9. A pad must be drawn to the board to connect the antenna via short coaxial cable. The "PRG" connector and R1 are connected to enable future firmware updates. The serial interface is connected to the USART of the MCU. Resistors R14 and R15 lower the received serial signal to the level of the used Vcc from 5 V to 3.3 V with a regular voltage division circuit. Resistors R16 to R18 are optional and are installed if the MCU's decision level is not reached with the 3.3 V serial signal. In this case the line over R18 must be cut. The option to put a DC level to the signal was found unnecessary in prototyping. The radio module is surrounded with grounded through-PCB vias to prevent noise on the radio frequency.

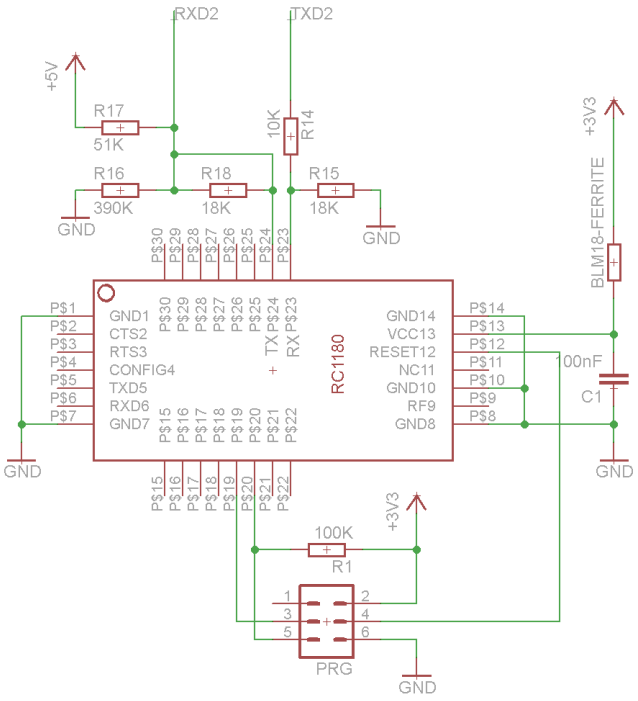

Figure 32. The schematic of the connections of the Mains sensor's radio module.

4.1.5. Power Supply

The Vcc:s are supplied to the device with an AC – AC adaptor having two separate secondary coils that provide 8 V and 22 V AC voltages. The Vcc to the MCU and to the radio module are both fed from the 8 V AC input via rectifier and parallel 5 V and 3.3 V LP2985 type regulators [56, 57]. The 10 µF bypass capacitors are used as suggested in the datasheet to reduce the output noise. Input capacitor at least of 1 µF and output capacitor at least of 2.2 µF are required to ensure the stability of the regulator. These capacitors can be increased without upper limit so 100 µF and 470 µF surface mountable capacitors are used since they were physically small enough to fit in the selected casing. They will also act as energy storage to be able to service especially the radio module during transmission which can involve power surges.

The amplifier is powered with the other secondary coil. The power circuit has its own rectifier of the same type as the other circuitry and a 18 V regulator [58]. The regulator is stabilized in the same manner with bigger than required 100 µF capacitors and an IC protective diode is installed from output to input as suggested in the datasheet. This ensures that the input voltage will never be more than 0.7 V lower than output voltage, which prevents possible damage to the regulator. Since the positive Vcc of the amplifier is 18 V and the negative is 0 V, the virtual ground used to the signal must essentially be the same as the GND of the ADC. A precision virtual ground IC could be used but since most inaccuracies come from the ADC and the VCC of the amplifier is regulated, regular voltage division is considered to be adequate [59]. Both divided voltages have their own capacitors to stabilize the action.

4.1.6. PCB Layout

The layout of the PCB fits in the Hammond Manufacturing 1593N casing [60]. A double-sided PCB was engineered using as much as possible surface mountable components. Any unused surface of the PCB is made a ground level. The handmade prototype is shown in Figure 33.

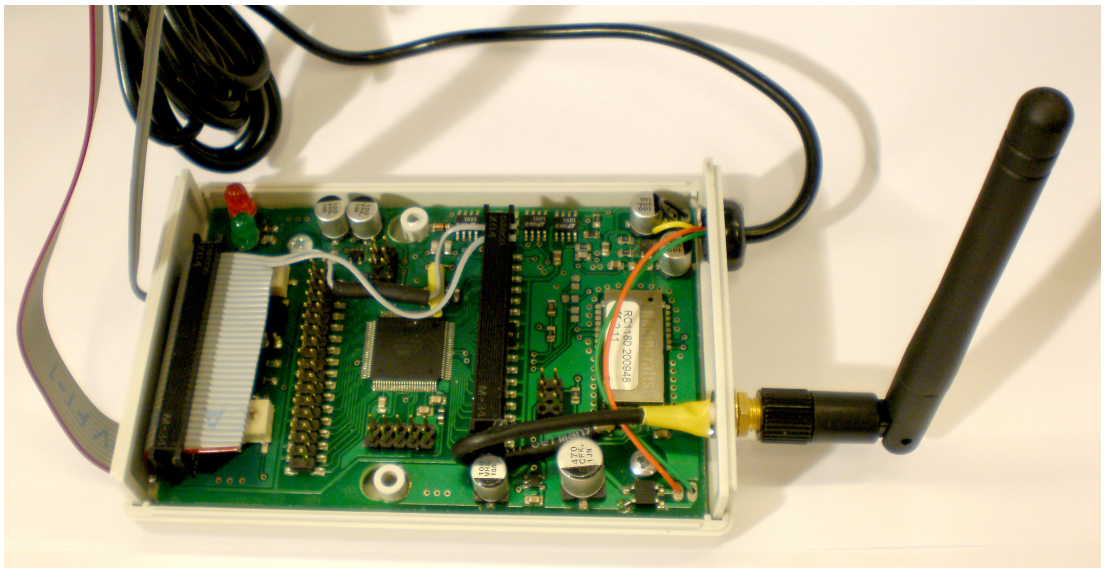

Figure 33. The Mains sensor hardware.

4.2. Software

4.2.1. Overview

The software was implemented by updating the previous version of the UBI-AMI sensor software and incorporating the changes required by the new MCU. The software is programmed in C using Atmel's libraries and integrated development environment (IDE). The UART library was changed and some registers were updated to match the new MCU.

The software consists of 4479 lines of code divided into eight source files named "calibrate", "chooseSensor", "coap", "debug", "nap", "runtime_update", "socket_sensor" and "usart". "calibrate" and "chooseSensor" are completely new source codes specific to the Mains sensor. Changes were also made to "usart" and "socket_sensor".

"socket_sensor" contains the "mains" function as well as functions for measuring, calibrating and communicating using the CoAP protocol as well as all basic functionalities of the device. "calibrate" is for calibrating the sensor and for some options, "chooseSensor" is simply mapping I/O's to the Hall sensors so they can be chosen and closed with a simply command, "coap" is the communication library, "debug" is for printing debug messages in hexadecimal form via UART, "nap" is the closed source interface of the radio module, "runtime_update" is for flashing at runtime when con-

tinuations are used, and "usart" is the library for the UARTs. An example of the source code is included in appendix A.

Flashing a sensor at runtime would cause undefined loss of data. It is not used in the current design, but it could be possibly enforced at every start up in future designs. The library exists for compatibility reasons since the SW can be translated with minor changes to other platforms.

The time critical parts of the SW are triggered by interrupts. The reading of the measurements saves the test output data to the EEPROM, reads the value of one Hall sensor and calculates temporary total consumption. The semaphore to read the measurements is raised once in a second in the ISR.

4.2.2. Software for Pulse Inputs

The SW of the previous version was originally designed for both the mains sensor and the socket sensor. The mains sensor had a pulse input for the optical test output of the kilowatt hour meter and the socket sensor had a pulse input for the measuring circuit. These were connected to different I/O's of the MCU, but to the same interrupt vector. The same approach is used to connect both pulse inputs to the same interrupt vector. The names of the I/O's, registers and interrupts were changed and the timing of the interrupts was fine-tuned to improve the reliability of the measurement. The values of the pulse inputs are calculated every 30 seconds by reading the previous value from the EEPROM and subtracting it from the current value of the pulses. The resulting number of pulses is multiplied by a value calibrated to the EEPROM to determine the total energy consumption over the last 30 seconds.

The external interrupt for the pulse inputs is connected to the port J pins 4 and 5 of the MCU [48]. These I/O's have the capability for the "pin change interrupt", which means that it will be triggered whenever the state of the input pin changes. The initialization of the interrupt is located in the "initMain" function. Pull-ups are set for both pins leaving less room for possibly adjusting the potentiometer of the optical input, thus the potentiometer should be adjusted to its most resistive position. The interrupt routine is the same for both pulse inputs. There is a simple flip-flop in the code to remember the old state of the input, in order not to trigger the interrupt twice on one pulse and a short timer overflow interrupt is used to disable the external interrupts until the possibly built-up transient is over from the pulse. Using a short timer instead of a delay is an optimization, as it does not reserve time from the arithmetic logic unit (ALU) except the actual ISR, but is run parallel on the clock tree, leaving as much as possible of the constrained resources of the MCU unused.

The EEPROM is guaranteed by the manufacturer to be re-writable 100,000 times. Since the measurement of the total energy consumption is saved every second the place to write must be altered in order to use the meter uncorrupted for over 28 hours. The minimum recording time is 1500 hours yielding 5,400,000 32-bit measurements which total 21,600,000 bytes that clearly cannot fit in the 4 KB EEPROM of the MCU. The workaround is to use a ring buffer in order not to having add external memory to the device. This way the whole area of the ring buffer is at use in rewriting the measurements. The ring buffer reserves addresses from 113 to 2752 for 660 32-bit numbers, which yield minimum functional time of 1833 hours. This represents 659-fold im-

provement over writing just at one place. Efficiency is further increased by updating only differing bits instead of clearing and rewriting the whole value. The rest of the EEPROM from address 2753 to 4072 is used as an address pointer register, e.g. status buffer, while using the ring buffer. The ring buffer was implemented according to [61]. It was first programmed on a PC using the ANSI-89 version of the C language and the working program was then converted to the ATmega platform. The EEPROM must be initialized before using the ring buffer to ensure the reliability of the status buffer.

4.2.3. Software for Hall Sensors

The reading of the Hall sensors is done in the "measureFuse" function as follows:

- A Hall sensor is chosen to be measured. A state variable is used to match each connected sensor head. It cycles through the values from the first to the last calibrated Hall sensor over and over again. The equivalent sensor head is selected using the "chooseSensor" function.
- After a short delay the amplifier is started by disconnecting the grounding of the sample circuit.
- The ADC operation is enabled on the registers and conversions started. The first conversion is ignored as protection against possible errors in certain situations. The value of the second conversion is used in load calculations.
- The value of the measurement is calculated using calibrated values of the level of basic noise and the Hall sensor specific calibration value multiplier if the calibrated noise floor is surpassed. The value is rounded to full watts and saved to the measurement table.
- The opened sensor head connection is closed and the measurement amplifiers sample circuit is reset again.

The ADC is initialized in the "initADC" function. First, the ADC is disabled before setting register values. The sample of the amplifier is cleared and left connected to GND. The reference voltage is set to be external voltage on pin "AVCC" of the MCU with a capacitor on "AREF" pin, the ADC channel is set to "ADC0", the single ended input with zero gain is selected and the right adjusted result is left untouched in "ADMUX" register. The values of the ADC are read in the "measureFuse" function. The function is called once in a second but a different Hall sensor is chosen at each time. This way the values are updated into the measurement table the more often the fewer sensors are connected.

4.2.4. Programming Interface for Debugging and Calibration

The MCU provides an UART serial interface for receiving commands and sending resulting messages. The UART can be connected to a PC's serial port using UART - RS232 level shifter or to an USB port using UART - USB converter circuit and

virtual serial port driver. The programmer can use a simple UI to write debugging and calibration commands and to view resulting messages. Available commands and their parameters are listed in Table 2.

Table 2. Commands for the calibration using programmers UI

Command	Action
#a	Amount of sensors
#b	Blinks: 3600 for 100 blinks/kWH, 360 for 1000 blinks/kWH, 36 for 10 000 blinks/kWH and 750 for 480 blinks/KWh
#c	Compensation on/off (1/0), use off if not connected to the pulse input
#s1...#s30	Calibration multiplier to the sensor
#n	Value for the floor noise
#r	Not in use, future option

4.3. UBI-AMI version 2.0

The UBI-AMI version 2 comprises of a WSN router, a Mains sensor and one or more Socket sensors shown together with a demo circuit panel in Figure 34 [62].

The WSN router is a proprietary device provided by Sensinode. With quarter wave antennas the router is supposed to have 500-600 m LOS (line of sight) wireless range.

There are two types of sensors, the Mains sensor designed in this thesis and the Socket sensor designed in Pauli Närhi's M.Sc. thesis [63].

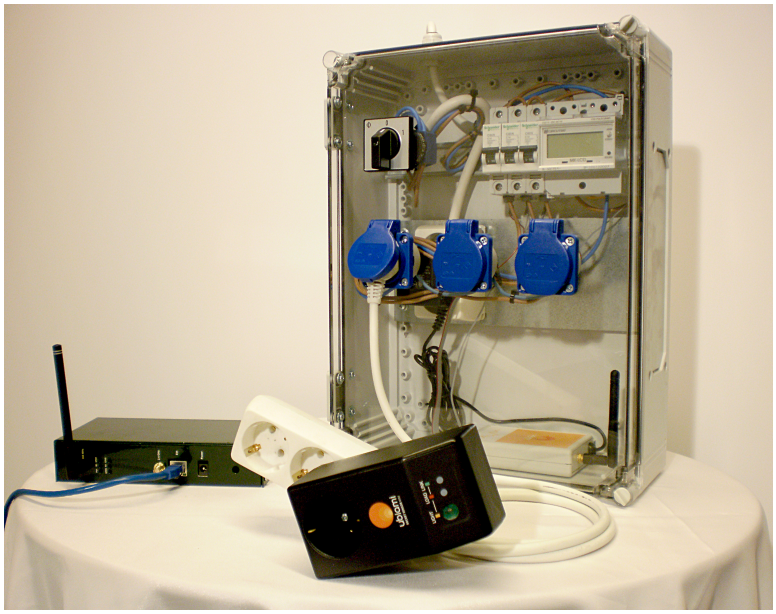

Figure 34. The demosetup of the whole system consists of the green router on the left, the socket sensor connected to the extension chord on the front and the demo switchboard with the kilowatt hour meter on the back containing the orange labeled Mains sensor on the bottom and the Hall sensors taped under each fuse.

Figure 35 shows an example of the web-based user interface where the total energy consumption is visualized with four gauges corresponding to euros and kWh and their relative changes with respect to the previous values.

Figure 35. A screen capture of the new UI on the web browser.

5. EVALUATION

The annex F of the international standard IEC62052-11:2003 provides a list of recommended test sequences for electricity metering equipment. The list contains 26 different tests addressing various properties such as accuracy, insulation, EMC, climatic effects and mechanics. Since the prototype uses safe voltages and the reliability of the data transfer is tested separately in field tests, testing in this thesis is limited to the accuracy of the measurement. The tests are executed according to the standard when applicable.

5.1. Functional Evaluation

The Mains sensor has optical and galvanic inputs for the test output of the kilowatt hour meter and connections to 30 Hall sensors. Thus, it can measure the aggregate load as well as the loads of 30 individual fuses in the circuit breaker panel. An example of the part of a load tree covered by a Mains sensor is presented in Figure 36. The Mains sensor enables isolating the energy consumption of an integrated appliance from the total consumption. However, if multiple integrated appliances of similar consumption are connected in the same group, they cannot be separated with the Mains sensor which regards them as one appliance being on with half or full power. Extra means such as connecting another Mains sensor to the wires of these appliances is needed to achieve full coverage. In any case, we can conclude that the Mains sensor fulfills the functional requirements set in Chapter 3.

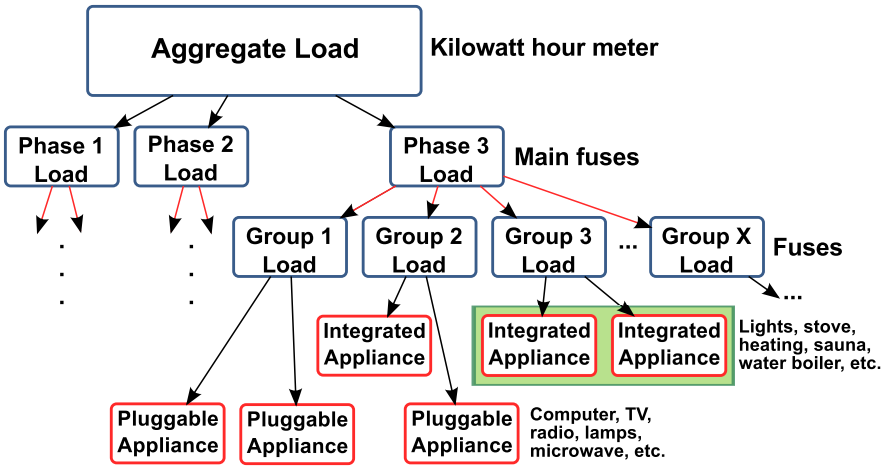

Figure 36. Load Tree: green area is marking two integrated appliances of same size locating in the same group, that can not be separated from each other.

5.2. Accuracy of Pulse Inputs

The theoretical accuracy of the Mains sensor is 100 % for the galvanic pulse input since it should not miss a pulse. The optical pulse input should be able to do the same in

ideal case. Testing would be very time consuming using real kilowatt hour meters, so a simple pulse generator was manufactured for testing purposes. It has an open collector output similar to the kilowatt hour meter in the demo switchboard used in testing and the waveforms are programmable [64]. A random number generator is used to create pulses with on/off time from 30 ms to 100 ms with galvanic connection and from 200 µsto 1 ms for the optical input [45]. The fastest signal gives maximum frequency of 2,500 Hz and it is also tested through the galvanic pulse input for the possibility of connecting an external optical pulse detector to it. The tests were executed using the same software for both inputs leaving only the input circuitry as variable.

The results for the galvanic input are presented in Table 3 and for the optical input in Table 4. The galvanic input was able to detect all 450 000 pulses with 100 % success rate. However, the optical input had errors. The circuitry copied from the previous version missed about 16

Table 3. Results of the tests of the galvanic pulse input:

Pulses Sent	Pulse Duration	Pulses received	Success Rate
10000	30 ms - 100 ms	10000	100 %
10000	30 ms - 100 ms	10000	100 %
10000	30 ms - 100 ms	10000	100 %
3 x 100000	30 ms - 100 ms	300000	100 %
4 x 3 x 10000	200 us - 1 ms	120000	100 %

Table 4. Results of the tests of the optical pulse input:

Pulses Sent	Pulse Duration	Pulses received	Success Rate
10000	30 ms - 100 ms	10425	104.25 %
4 x 3 x 10000	200 us - 1 ms	100830	84.025 %

5.3. Accuracy of Hall Sensors

5.3.1. Theoretical Accuracy

When the theoretical accuracy of the current measurement with the Hall sensors is calculated, three sources of error have to be considered: the Hall sensor itself, the measurement amplifier including the peak value detector, and the ADC. According to the datasheet, the maximum error of the Hall sensor (δ_H) is 0.3 % within range of the $\pm$16 A. The nonlinearity of the measurement amplifier (δ_A) is calculated by multiplying the output value of the 1 A measurement by 16 and comparing the result to the output value of the 16 A measurement simulation:

$$\delta_A = \frac{16 * 0.295886V - 4.72968V}{4.72968V} * 100\% = 0.09506\% \approx 0.1\% \qquad (7)$$

The accuracy of the ADC is ±2 LSB of the 10-bit range. It is relatively more inaccurate when small values are measured. Therefore, it is tested with the 1 A reference current of the standard EN50470-1:2006 [44]. It is one sixteenth of the range value of the ADC at 4.72968 V, so we can find out the nonlinearity of the ADC (δ_B) in the worst case scenario in a reasonable measurement range:

$$\delta_B = \frac{2}{\frac{1023 * \frac{4.72968V}{5V}}{16}} * 100\% = 3.30684\% \approx 3.307\% \quad (8)$$

The maximum total error (δ_T) is calculated according to the standard EN50470-3:2006 Annex A [65] as the quadrature sum of the three error components:

$$\delta_T = \sqrt{\delta_H^2 + \delta_A^2 + \delta_B^2} * 100\% = \sqrt{0.003^2 + 0.001^2 + 0.03307^2} * 100\% \quad (9)$$
$$= 3.32192\% \approx 3.33\%$$

Most of the error is due to the ADC when small currents are measured and the error will minimize on maximum values. The standard EN50470-3 lists the maximum permissible errors (MPE) for different types of meters. The estimated error of 3.33 % is sufficient for class A meters.

The lines between the Hall sensors and the measurement amplifier should be kept as short as possible to avoid EMC. The nonlinearity is the main concern in accuracy since the possible off-set can be calibrated off with the SW. The measurement of the energy consumption of integrated elements of the household is therefore carried out with sufficient accuracy.

5.3.2. Experimental Accuracy

Three tests were conducted to compare the energy consumption measurements of the Hall sensors against to the output of the kilowatt hour meter of the demo switchboard. The tests were done according to the standard "as is" without any result improving algorithms or calibration. The standard defines 1 A, 2 A and 5 A currents to be used in the tests [44]. They are more than enough for finding out if the required minimum 1 A current is present. The loads used in the tests consist of eight lamps in the office, due to the lack of reference loads and reference meter. Their currents are of wider range than required in the standard which is only considered beneficial due to the wider range of tested values. It should be noted that the AC voltage was not constant but varied between 222 VAC and 229 VAC during the tests according to the kilowatt hour meter. Also, the temperature of the office was not controlled and could have had an effect to the measurements.

As seen from Table 5, the calibration was 0.87 % low. When this offset is taken into account, the average accuracy of the Hall sensors against the commercial kilowatt hour meter was ± 0.47 % in all three tests. The calibration is a simple multiplication so it can be as well done on paper and there is no need to repeat the tests. The second test conducted during office hours has the worst deviation of the sample values. The spurs of up to 2835 W were actual measurements and could be repeated by switching on the lights or a coffee maker in the office. They would not have effect on the longer term measurement due to their short lifetime.

The sample data of the second test is used to explore a possible algorithm for removing spurs (Figure 37). The sample data is filtered by a simple moving window where the middle value of three consecutive samples is always selected. This removes spurs without changing the average value significantly although it increases the response time of the measurement. This algorithm is not included in the SW of the Mains sensor.

Table 6 shows the results of testing the relative accuracy of the Hall sensors with different loads. Each load was tested with three sensors to confirm relative consistency between sensors. One sensor was tested without a load over a longer period of time to verify that no false loads would show up without a load. We can see that the values are consistent with each other and with the loads, thus confirming the functionality of the measurement.

Reactive power was measured with the Hall sensors in two tests. 1% increase was detected when the load was fed through transformer resulting to the better visibility of the active power.

Table 5. Results of the testing the Hall sensors against commercial kilowatt hour meter with a 7 A load:

Samples (pcs)	Avr (W)	Min (W)	Max (W)	Reference (W)	Accuracy (%)
16,411	1467	1411	1512	1487	98.66 %
14,371	1481	1411	2835	1487	99.60 %
14,681	1469	1411	1512	1480	99.26 %

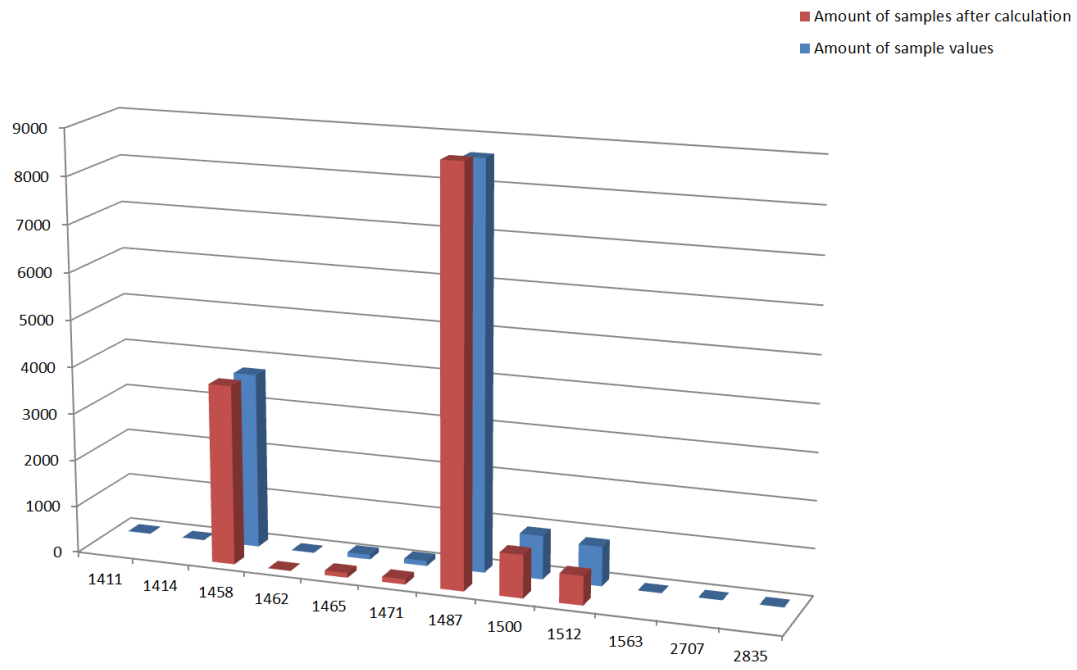

Figure 37. The sample deviation of the Hall sensors. Original samples are shown with the blue bars, filtered results are shown with red bars.

Table 6. Results of the tests of Hall sensors with differend loads:

Load (A)	Samples	Average (W)	Min (W)	Max (W)
1	622	192	187	212
1	606	192	187	212
1	627	190	187	212
3	638	769	750	775
3	648	772	750	775
3	656	773	750	775
7	612	1489	1411	1512
7	505	1490	1411	1512
7	624	1500	1411	1512
0	2606	0	0	0

5.4. External Interfaces

Considering the initial requirements set for external interfaces, we can make the following observations:

1. The measurement of the pulses of the total load reaches up to 362,250,000 pulses using 32-bit ring buffer. Optical pulses can be recognized with the used phototransistor, but input circuitry should be redesigned to improve accuracy.

2. The Mains sensor is capable of measuring up to 30 electrical groups from the fuse board using only safe voltages in measurement heads.

3. The JTAG programming interface allows programming the MCU. The USART interface is used to calibrate and configure the settings of the sensor. A separate programming interface was implemented for the radio module.

4. The SW can be debugged via the JTAG interface. Additional USART interface can be used to receive debugging messages and two LEDs are to indicate the state of the sensor.

5.5. Future Development Opportunities

The evaluation showed that the Mains sensor fulfills the requirements. However, the device could be improved further in several ways.

In terms of measurement technologies, the optical pulse input circuitry should be redesigned since the current design adopted from the Mains sensor version 1 was found to be inaccurate. Further, digital measurement devices could be used to achieve better accuracy in measuring the loads of the fuses. Even real active power measurement could be supported at the cost of increased intrusiveness to the fuse board of the household. Alternatively, to minimize intrusion, the power signatures of individual appliances could be extracted from fuse specific data to identify individual appliances and to isolate their energy consumption.

In terms of communications, the wireless communication technology used in this prototype proved problematic due to the lack of functional radio modules and routers, and the poor reliability and range of the wireless links. At the time no other 6LoWPAN compatible products were available. Alternatively, KNX or SPI could be considered for data communications.

The sensor software could also be improved. Especially, the use of the serial ports could be enhanced not to block more time critical parts of the system.

6. CONCLUSION

The objective of this thesis was to design and implement a new Mains sensor to the UBI-AMI system version 2 that would provide more comprehensive view on domestic energy consumption than the Mains sensor of the UBI-AMI version 1. The sensor was designed to measure the aggregate load from the test output of a kilowatt hour meter using either optical or galvanic pulse input. The loads of integrated appliances are measured from the circuit board using Hall sensors. The sensor uses the 6LoWPAN protocol stack with IEEE 802.15.4 radios in the sub-GHz band and the CoAP protocol for transmitting the sensor data to the UBI-AMI server.

The hardware involved selecting appropriate measurement technologies such as the Hall sensors, simulating analog components such as the input circuitries, selecting suitable digital components such as the MCU, and designing the PCB for housing all the components. The software was based on the UBI-AMI version 1 with redesigned and fine-tuned measurement functions and new interfaces for programming and debugging purposes. The sensor was designed to survive power outages without losing calibration and measurement data that are stored in the EEPROM of the MCU. The measurement data is written into the EEPROM using a ring buffer, which provides sufficient capacity and extends the lifetime of the EEPROM.

The Mains sensor was experimentally evaluated with a commercial kilowatt hour meter and a pulse generator. The galvanic pulse input was able to read the test pulse sequence without a single error, whereas the optical pulse input based on the version 1 input circuitry missed a portion of fast pulses and oversampled slow pulses. The Hall sensors were found to have $\pm$ 0.47 % average error compared to the commercial kilowatt hour meter. In conclusion, the Mains sensor was found to meet the functional and performance requirements set at the beginning of the project, and it provides sufficiently accurate and reliable information for improving the awareness of energy consumption of a household.

7. REFERENCES

[1] (cop. 2011) Buildings Energy Data Book. U.S. DOE.

[2] (cop. 2003) Commercial buildings energy consumption survey. U.S. DOE.

[3] Bertoldi P. & Atanasiu B. (cop. 2006) Electricity consumption and efficiency trends in the enlarged European Union. European Commission Report EUR 22753.

[4] Chetty M., Tran D. & Grinter R.E. (2008) Getting to green: Understanding resource consumption in the home. 242 p. ID: SCOPUS4; ID: Scopus.

[5] Stern P. (1992) What psychology knows about energy conservation. American Psychologist 47, pp. 1224–1232.

[6] Shelby Z. & Bormann C. (cop. 2009) 6LoWPAN: The Wireless Embedded Internet. Wiley.

[7] Ojala T., Närhi P., Leppänen T., Ylioja J., Sasin S. & Shelby Z. (2011) Ubi-ami: Real-time metering of energy consumption at homes using multi-hop ip-based wireless sensor networks. In: Proc. GPC2011, Oulu, Finland.

[8] Lifton J. (2007) A platform for ubiquitous sensor deployment in occupational and domestic environments. ID: ACM; ID: ACM Digital Library.

[9] Zigbee (accessed 12.09.2014). URL: http://www.zigbee.org.

[10] Hart G.W. (1992) Nonintrusive appliance load monitoring. 1870 p. URL: http://goo.gl/yqNup.

[11] Google powermeter (accessed 06.09.2011). URL: http://www.google.org/powermeter.

[12] Microsoft hohm (accessed 30.01.2012). URL: http://www.makeuseof.com/dir/microsofthohm-reduce-home-energy-costs/.

[13] Fortum kotinäyttö (accessed 30.10.2014). URL: http://www.fortum.com/countries/fi/yksityisasiakkaat/energiansaasto/kauppa/fortum-kotinaytto/pages/default.aspx.

[14] Knx, cenelec en 50090 and cen en 13321-1 (accessed 12.10.2014). URL: http://www.knx.org/knx-standard/introduction/.

[15] Usman A. (2013) Evolution of communication technologies for smart grid applications. Renewable and Sustainable Energy Reviews 19, pp. 191–199. ID: SCIDI4; ID: ScienceDirect (Elsevier).

[16] Iwansson K., Sinapius G. & Hoornaert W. (cop. 1999) Measuring current, voltage, and power. Elsevier, Amsterdam, xv, 216 s p.

[17] Microchip mpc3909: Energy metering ic with spi interface and active power pulse output, (accessed 12.06.2014). URL: http://www.microchip.com/wwwproducts/Devices.aspx?dDocName=en520376.

[18] Ramsden E. (c2006) Hall-effect sensors : theory and applications. Elsevier/Newnes, Amsterdam, 2nd ed. ed.

[19] Middelhoek S. & Audet S.A. (1989) Silicon sensors. Academic Press, London, 376 s p.

[20] Echun electronic co. ltd (echun) ecs1030-l72: Datasheet (accessed 12.08.2014). URL: http://dlnmh9ip6v2uc.cloudfront.net/datasheets/Sensors/Current/ECS1030-L72-SPEC.pdf.

[21] Beijing yaohuadechang electron co.,ltd (yhdc) sct-013: Datasheet. URL: http://www.sparkfun.com/datasheets/Sensors/Current/2009511142810295.gif.

[22] Fluke: i3000s flex ac current clamp (accessed 02.06.2014). URL: http://www.fluke.com/fluke/usen/accessories/Current-Clamps/i3000-Flex-4PK.htm?PID=56293.

[23] Isolated current and voltage transducers: Charasteristics, applications, calculations (accessed 12.05.2014). URL: http://www.lem.com/images/stories/files/Products/P1_5_1_industry/CH24101E.pdf.

[24] Thomson W., On the electro-dynamic qualities of metals: Effects of magnetization on the electric conductivity of nickel and iron, "proc. roy soc., vol. 8, pp 546-550, 1857.

[25] Potter R. (1975) Anisotropic magnetoresistance in ferromagnetic 3d alloys. IEEE Transactions on Magnetics 11, pp. 1018–1038. ID: PQ_MS; ID: Advanced Technologies Database with Aerospace (ProQuest).

[26] Baibich M.N., Broto J.M., Fert A., Dau F.N.V., Petroff F., Eitenne P., Creuzet G., Friederich A. & Chazelas J. (1988) Giant magnetoresistance of (001)fe/(001)cr magnetic superlattices. Physical Review Letters 61, p. 2472. ID: SCOPUS4; ID: Scopus.

[27] Reig C., Cubells-Beltrán M. & Muñoz D.R. (2009) Magnetic field sensors based on giant magnetoresistance (gmr) technology: Applications in electrical current sensing. Sensors 9, p. 7919. ID: SCOPUS4; ID: Scopus.

[28] Ramirez A.P. (1997) Colossal magnetoresistance. Journal of Physics Condensed Matter 9, p. 8171. ID: SCOPUS4; ID: Scopus.

[29] Lee L.P., Longo J., Vinetskiy V. & Cantor R. (1995) Low-noise yba2cu3o7-d direct-current superconducting quantum interference device magnetometer with direct signal injection. Applied Physics Letters , p. 1539ID: SCOPUS4; ID: Scopus.

[30] Dargie W. & Poellabauer C. (2010) Fundamentals of wireless sensor networks : theory and practice. Wiley, Chichester, West Sussex, U.K. Includes index.

[31] Ieee computer society, "ieee std. 802.15.4-2003", october 2003.

[32] Hersent O., Boswarthick D. & Elloumi O. (cop. 2012) The Internet of things : key applications and protocols. Wiley-Blackwell, Chichester.

[33] Ietf rfc4919: Ipv6 over low-power wireless personal area networks (6lowpans): Overview, assumptions, problem statement, and goals .

[34] Ietf rfc4944: Transmission of ipv6 packets over ieee 802.15.4 networks .

[35] Plugwise smart meter system (accessed 12.10.2014). URL: http://www.plugwise.com/idplugtype-f/.

[36] Radiocrafts rc2301 (accessed 03.09.2014). URL: http://www.radiocrafts.com/uploads/rc230x_data_sheet_1_2.pdf.

[37] Montenegro G., Kushalnagar N., Hui J. & Culler D. Transmission of IPv6 packets over IEEE 802.15.4 networks. IETF RFC 4944.

[38] Sensinode nanostack 2.0 (accessed 12.06.2014). URL: http://www.sensinode.com/EN/products/software.html.

[39] Linksys wrt54gs (accessed 12.06.2014). URL: http://downloads.linksysbycisco.com/downloads/datasheet/1224638902575/wrt54gs_ds_2.pdf.

[40] Kamikaze openwrt (accessed 12.07.2014). URL: http://kamikaze.openwrt.org/7.09/.

[41] Aberer K., Hauswirth M. & Salehi A. (2006) A middleware for fast and flexible sensor network deployment. In: 32nd International Conference on Very Large Databases, pp. 1199–1202.

[42] Mysql (accessed 12.05.2014). URL: http://www.mysql.com.

[43] Glassfish (accessed 12.05.2014). URL: http://glassfish.java.net.

[44] En 54070-1:2006 , pp. 21–22.

[45] Iec62052-11:2003 , pp. 45–47.

[46] Iec62053-31:1998 , pp. 6, Annex B, C.

[47] Radiocrafts rc1180 datasheet (accessed 12.10.2014). URL: http://www.radiocrafts.com/uploads/rc11xx-rc232_data_sheet_1_44.pdf.

[48] Atmel atmega2560 datasheet (accessed 12.10.2014). URL: http://www.atmel.com/images/doc2549.pdf.

[49] Ietf draft: Constrained application protocol (coap) draft-ietf-core-coap-14 (accessed 21.08.2014), http://tools.ietf.org/id/draft-ietf-core-coap-14.txt .

[50] Nec - ps2561al-1-e3-a optoisolator datasheet (accessed 12.10.2014). URL: http://www.cel.com/pdf/datasheets/ps2561a.pdf.

[51] On semiconductor mmbt3904lt1 datasheet (accessed 12.10.2014). URL: http://www.onsemi.com/pub_link/Collateral/MMBT3904LT1-D.PDF.

[52] Motorola mrd14b cascade phototransistor datasheet (accessed 12.10.2014). URL: http://www.datasheetarchive.com/MRD14B-datasheet.html.

[53] Cslt6b100 hall sensor's datasheet (accessed 12.10.2014). URL: http://sensing.honeywell.com/index.php/ci_id/49803/la_id/1/document/1/re_id/0.

[54] Linear lt1001 operational amplifier datasheet (accessed 12.10.2014). URL: http://cds.linear.com/docs/en/datasheet/1001fb.pdf.

[55] Sedra A.S. & Smith K.C. (2010) Microelectronic circuits. Oxford University Press, New York, 6th ed. ed., N. 1450 s p.

[56] Fairchild semiconductor mb1s bridge rectifier datasheet (accessed 21.08.2014). URL: http://www.fairchildsemi.com/ds/MB/MB8S.pdf.

[57] Texas instruments lp2985 datasheet (accessed 12.10.2014). URL: http://www.ti.com/lit/ds/symlink/lp2985-n.pdf.

[58] Toshiba ta78l18 regulator datasheet (accessed 12.06.2014). URL: http://www.toshiba.com/taec/components2/Datasheet_Sync/265/5675.pdf.

[59] Texas instruments tle2426 precision virtual ground datasheet (accessed 12.06.2014). URL: http://www.ti.com/lit/ds/symlink/tle2426.pdf.

[60] Hammond manufacturing 1593n casing datasheet (accessed 14.08.2014). URL: http://www.hammondmfg.com/pdf/1593N.pdf.

[61] Application note: Avr101: High endurance eeprom storage (accessed 12.08.2014). URL: http://www.atmel.com/images/doc2526.pdf.

[62] Leppänen T., Ylioja J., Närhi P., Räty T., Ojala T. & Riekki J. (2012) Holistic energy consumption monitoring in buildings with ip-based wireless sensor networks. In: Proceedings of the Fourth ACM Workshop on Embedded Sensing Systems for Energy-Efficiency in Buildings, BuildSys '12, ACM, New York, NY, USA, pp. 195–196. URL: http://doi.acm.org/10.1145/2422531.2422567.

[63] Närhi P. (2014) Langaton energiankulutusmittari ipv6-pohjaiseen sensoriverkkoon. diplomityö. oulun yliopisto, tieto- ja sähkötekniikan osasto, oulu.

[64] Circutor kilowatt hour meter datasheet (accessed 12.06.2014). URL: http://www.circutor.com/docs/ft_m3_gb-mk-lcd.pdf.

[65] En 54070-3:2006 , pp. 8–19, Annex A.

8. APPENDICES

Appendix A: A Code Example

Appendix A: A Code Example

```
/*****************************************************
*
* calibrate.c
*
*****************************************************/

//#include <avr/io.h>
//#include <avr/interrupt.h>
//#include <avr/pgmspace.h>
#include <avr/eeprom.h>
#include <string.h>
#include "socket_sensor.h"
#include "calibrate.h"
#include "usart.h"

extern uint8_t command[21];
extern uint8_t n1;//command table pointer
extern uint8_t valueNeeded;//flag to collect value
extern uint8_t commandOngoing;
extern int amount_of_resources;//All resources
extern int pulseInputMultiplier;
extern int reactivePowerCompensation;
extern int noiseLevel;
extern int sensorCalibrations[31];
extern int seconddigit;
static volatile int addr;

static volatile int commandNumericValue = 0;

  char parseCommand(){
    seconddigit=0;
    char a = 0;
    //Amount of sensors
    if(!(strncmp(command, "#a", 2))) a = 1;
    //Blinks/kWH
    if(!(strncmp(command, "#b", 2))) a = 2;
    //Compensation of reactive power on/off
    if(!(strncmp(command, "#c", 2))) a = 3;
    //Noise value without load
    if(!(strncmp(command, "#n", 2))) a = 4;
    //New address for RD (Not in use.)
    if(!(strncmp(command, "#r", 2))) a = 5;
    //Sensor calibration value
    if(!(strncmp(command, "#s", 2))) a = 6;

      int decademultiplier=1;
      int i=0;
        //Reads amount of chars
        while((command[i+2] != 0x0D) && (i<6)){
        i++;
        }

        //char to int
        while(i> 0){
```

```
        seconddigit=seconddigit+((command[i+1]-48)
          *decademultiplier);
        i--;
        decademultiplier=decademultiplier*10;
        }

      commandNumericValue = seconddigit;
      seconddigit=0;

return(a);
}

void calibrateAmountOfSensors(int commandNumericValue){
  //assuring value 1-30
  if(commandNumericValue<1) commandNumericValue=1;
  if(commandNumericValue>30) commandNumericValue=30;
  //"all" resource counted in +1, mains = 0 hallsensors =
 commandNumericValue
  amount_of_resources = commandNumericValue + 1;
  eeprom_busy_wait();
  eeprom_update_word (( uint16_t *) EEPROM_ADDR_amountOfResources,
   amount_of_resources );
  usart1_puts_p(PSTR(" sensoria\n\r"));
}

void calibratePulseInput(int commandNumericValue){
  pulseInputMultiplier = commandNumericValue;
  eeprom_busy_wait();
  eeprom_update_word (( uint16_t *) EEPROM_ADDR_BlinksPerKWH,
    pulseInputMultiplier );
  usart1_puts_p(PSTR(" blinks\n\r"));
}

void calibrateReactivePower(int commandNumericValue){
  if (commandNumericValue != 0){
     reactivePowerCompensation = 1;
     usart1_puts_p(PSTR(" on\n\r"));
  } else{
      reactivePowerCompensation = 0;
      usart1_puts_p(PSTR(" off\n\r"));
    }
  eeprom_busy_wait();
  eeprom_update_word (( uint16_t *) EEPROM_ADDR_compensationOnOff,
   reactivePowerCompensation );
  usart1_puts_p(PSTR(" on\n\r"));
}

void calibrateNoiseValue(int commandNumericValue){
  noiseLevel = commandNumericValue;
  eeprom_busy_wait();
  eeprom_update_word (( uint16_t *) EEPROM_ADDR_NoiseValue,
 noiseLevel );
  usart1_puts_p(PSTR(" noise\n\r"));
}

void calibrateSensorHeads(int commandNumericValue){
```

```
  //parse value for sensor
  if (valueNeeded == 1){
    int seconddecademultiplier=1;
    int i=0;
    seconddigit = 0;
    //Reads amount of chars
    while((command[i] != 0x0D) && (i<6)){
    USART1_Transmit('\n');
    USART1_Transmit('\r');
    USART1_Transmit(command[i]);
    i++;
    }

    //char to int
    while(i> 0){
    seconddigit+= ((command[i-1]-48)*seconddecademultiplier);
    USART1_Transmit('\n');
    USART1_Transmit('\r');
    USART1_Transmit(command[i-1]);
    i--;
    seconddecademultiplier=seconddecademultiplier*10;
    }
    //assuring value 0-1000
    if(seconddigit<1) seconddigit=1;
    if(seconddigit>1000) seconddigit=1000;
    eeprom_busy_wait();
    eeprom_update_word (( uint16_t *) addr, seconddigit);
    USART1_Transmit('\n');
    USART1_Transmit('\r');
    //usart1_puts_p(PSTR(" add"));
    USART1_Transmit( 'a' );
    sensorCalibrations[(addr-EEPROM_ADDR_SensorCal)/2] =
      seconddigit;
    //usart1_puts_p(PSTR("ed\n\r"));
    USART1_Transmit( 'd' );
    valueNeeded = 2;
    addr = 0;
  }

  if (valueNeeded == 0){
    valueNeeded = 1;
    n1=0;
    addr = 0;
    //assuring value 0-30
    if(commandNumericValue<1) commandNumericValue=1;
    if(commandNumericValue>29) commandNumericValue=30;
    addr = EEPROM_ADDR_SensorCal + ((commandNumericValue-1) * 2);
    //usart1_puts_p(PSTR(" ?\n\r"));
    USART1_Transmit( '?' );
  }

  if (valueNeeded == 2) valueNeeded = 0;


}
```

```
void calibrateRD_Addr(int commandNumericValue){
}

//Actual calibrations
void calibrate(void){
  char a = parseCommand();
  switch(a){
    case 1: calibrateAmountOfSensors(commandNumericValue);
        break;
    case 2: calibratePulseInput(commandNumericValue);
        break;
    case 3: calibrateReactivePower(commandNumericValue);
        break;
    case 4: calibrateNoiseValue(commandNumericValue);
        break;
    case 5: calibrateRD_Addr(commandNumericValue);
        break;
    case 6: calibrateSensorHeads(commandNumericValue);
        break;
    default: usart1_puts_p(PSTR("\n\rSomething Wrong"));
  }
}
```